J. Physiol. (1980), **307**, *pp.* 97–129
With 15 *text-figures*
Printed in Great Britain

THE VARIANCE OF SODIUM CURRENT FLUCTUATIONS AT THE NODE OF RANVIER

BY F. J. SIGWORTH

From the Department of Physiology, Yale School of Medicine, New Haven, Connecticut 06510, U.S.A.

(*Received 11 July 1979*)

SUMMARY

1. Single myelinated nerve fibres 12–17 μm in diameter from *Rana temporaria* and *Rana pipiens* were voltage clamped at 2–5 °C. Potassium currents were blocked by internal Cs^+ and external tetraethylammonium ion. Series resistance compensation was employed.

2. Sets of 80–512 identical, 20 ms depolarizations were applied, with the pulses repeated at intervals of 300–600 ms. The resulting membrane current records, filtered at 5 kHz, showed record-to-record variations of the current on the order of 1 %. From each set of records the time course of the mean current and the time course of the variance were calculated.

3. The variance was assumed to arise primarily from two independent sources of current fluctuations: the stochastic gating of sodium channels and the thermal noise background in the voltage clamp. Measurement of the passive properties of the nerve preparation allowed the thermal noise variance to be estimated, and these estimates accounted for the variance observed in the presence of tetrodotoxin and at the reversal potential.

4. After the variance σ^2 was corrected for the contribution from the background, its relationship to the mean current I could be fitted by the function $\sigma^2 = iI - I^2/N$ expected for N independent channels having one non-zero conductance level. The single channel currents i corresponded to a single-channel chord conductance $\gamma = 6{\cdot}4 \pm 0{\cdot}9$ pS (S.D.; $n = 14$). No significant difference in γ was observed between the two species of frogs. The size of the total population of channels ranged from 20,000 to 46,000.

5. The voltage dependence of i corresponded closely to the form of the instantaneous current–voltage relationship of the sodium conductance, except at the smallest depolarizations. The small values of i at small depolarizations may have resulted from the filtering of high-frequency components of the fluctuations.

6. It is concluded that sodium channels have only two primary levels of conductance, corresponding to 'open' and 'closed' states of the channel.

7. The fraction p_{max} of channels open at the time of the peak conductance was found to be $0{\cdot}59 \pm 0{\cdot}08$ (S.D.; $n = 5$) and $0{\cdot}9 \pm 0{\cdot}1$ (S.D.; $n = 3$) for depolarizations to -5 and $+125$ mV, respectively. (50 ms hyperpolarizations to -105 mV preceded

Present address: Max Planck Institut für Biophysikalische Chemie, D-3400 Göttingen, Postfach 968, West Germany.

0022-3751/80/1710-0362 $07.50

the depolarizations in each case.) These values are similar to those predicted by Hodgkin-Huxley kinetics.

8. Fluctuations in the firing threshold of neurones are expected from the stochastic gating of sodium channels. A prediction of the size of these fluctuations based on the measured properties of the channels gives a value of about 1 % for the relative spread, which agrees with experimental values in the literature.

INTRODUCTION

The analysis of membrane current fluctuations has provided estimates for the unit conductance of many different ionic channels in axons, synapses and motor end-plates (see reviews by DeFelice, 1977; Neher & Stevens, 1977). Fluctuations in the sodium current of axons have been particularly difficult to analyse, however, because of their rapid kinetics and the spontaneous inactivation of the current. This paper and the succeeding one (Sigworth, 1980) describe a method of fluctuation analysis that removes the difficulty posed by inactivation, and present some basic results about the properties of single sodium channels.

This paper is primarily concerned with the number and size of the conductance levels of sodium channels. This kind of information would best be obtained by recording currents through single channels, as has been done recently in the acetylcholine receptor channel (Neher & Sakmann, 1976; Neher, Sakmann & Steinbach, 1978). No nerve preparation, unfortunately, has yet shown a sufficiently low noise level to resolve single sodium channel currents; instead, indirect methods have been used. Based on the assumption of two conductance levels for the channel (one of which is zero), estimates for the single-channel conductance have already been obtained by several means, including the analysis of membrane current fluctuations (see Conti, Hille, Neumcke, Nonner & Stämpfli, 1976*b*; and the review by DeFelice, 1977).

In their careful work using frog myelinated nerve, Conti *et al.* (1976*a*, *b*) also tested the assumption of two conductance levels by observing the voltage dependence of the single-channel conductance and by modifying the inactivation process in the channels. The work described in this paper extends the tests for additional conductance states to larger depolarizations and to conditions of higher membrane conductance. The experimental results are found to be consistent with two-conductance-state theories, and also allow the peak fraction of channels open (p_{max}) to be estimated.

I have used ensemble fluctuation analysis to study the sodium currents in the frog node of Ranvier. In this technique the membrane currents, elicited by successive, identical depolarizations, are recorded and the fluctuations within the ensemble of responses are analysed. The procedure is based on the one used by Lamb & Simon (1977) in their study of membrane potential fluctuations in photoreceptors. It differs from previous measurements of current fluctuations (see Neher & Stevens, 1977; Conti & Wanke, 1975) in not requiring stationarity of the membrane currents. It is ideally suited, therefore, to the study of conductances that change with time. Preliminary reports of this work have already been made (Sigworth, 1977, 1978).

METHODS

The experimental apparatus and procedures are described in the first part of this section. The node of Ranvier preparation was used in these voltage clamp experiments because of the low thermal noise level that can be obtained, and because the moderate number of sodium channels results in relatively large current fluctuations. From sets of current records, the mean time course, variance and autocovariance were calculated on a computer by a procedure designed to lessen the effects of long-term drifts. The voltage clamp system, which incorporates series-resistance compensation and a facility for measuring the internodal resistances, is described further in the Appendix. The second part of this section examines the contributions of various instrumental sources of fluctuations to the total ensemble variance. The largest undesired variance component was from thermal noise sources; its contribution was calculated explicitly to provide a correction to the total variance.

Preparation and voltage clamp

Single fibres of 12–17 μm diameter were dissected from the sciatic nerves of *Rana temporaria* (nodes 12–19) or northern *Rana pipiens* (nodes 21–43) by a technique similar to that described by Stämpfli & Hille (1976). No attempt was made to discriminate between motor and sensory fibres. After a fibre was mounted in the chamber and the internodal segments were cut in the end pools, the end pool solutions were immediately changed from Ringer to a 100 mM-CsCl, 20 mM-NaCl solution (nodes 12–36) or to a 120 mM-KCl solution (nodes 38–43). The first solution blocks the potassium current while maintaining the outward sodium current at large depolarizations. The solution bathing the node was potassium-free Ringer solution with tetraethylammonium ion (TEA) added to ensure sufficient block of the potassium current. Its composition was (concentrations in mM) 100 NaCl, 20 TEA-Cl, 2 $CaCl_2$ and 3·5 buffer, either Tris-HCl (nodes 12–19) or HEPES at pH = 7·4. The experiments were performed at temperatures in the range 2–5 °C.

The peak sodium currents observed in these fibres at -5 mV were in the range of 5–11 nA (see Table 1), corresponding to $\bar{P}_{Na}$ in the range $3–6 \times 10^{-10}$ cm^3 sec^{-1}. These values are lower by a factor of 2 or more than values previously reported in the literature even when the low temperature of these experiments is taken into account. The discrepancy may be partly due to the choice of the holding potential, -75 mV in these experiments as compared with -90 mV in the experiments of Conti *et al.* (1976). Ultra-slow inactivation (Fox, 1976; Neumcke, Schwarz & Stämpfli, 1979) may have reduced the current by as much as a factor of two in these experiments. Normal sodium currents for these species of frogs may also be smaller than reported previously. Hille (1971*a*) noticed what may be a large regional variation in $\bar{P}_{Na}$; also, many previous determinations of $\bar{P}_{Na}$ were not calibrated by the measurement of R_{ED} in the same fibres. In my work the low values of I_{Na} were seen consistently in more than thirty fibres. It should be noted that an earlier report (Sigworth, 1977, Fig. 1) shows, because of a mislabelled scale bar, peak currents of 15 nA. The peaks of the currents shown in the Figure were 7·5 nA.

The voltage clamp (Fig. 1) uses the original two-amplifier configuration of Dodge & Frankenhaeuser (1958) but incorporates many of the enhancements of Nonner (1969) and Hille (1971*a*). The nerve chamber is identical to that of Hille except for the addition of an integral, grounded, platinum-foil shield that contacts the *B* pool. An improved amplifier design allows fast response even with small fibres. The natural frequency of the voltage clamp loop ranges from 20 kHz with a 12 μm fibre to 100 kHz with a 17 μm fibre.

Two novel features of the voltage clamp are the facilities for series resistance compensation and for the measurement of the internodal segment resistances. Series resistance compensation is provided in the usual fashion by summing a portion of the current monitor signal with the command voltage. A low-pass filter prevents this positive feed-back from destabilizing the feed-back loop, so that it is possible to compensate entirely, and even overcompensate, for the series resistance in the preparation. Because this technique is applicable to other kinds of voltage clamps as well, its theoretical basis is detailed in the Appendix.

In most of the experiments reported here a fixed compensation of $0·01 \times R_{ED}$ was used, which corresponds to a series resistance value of about 0·3 M Ω in a 15 μm fibre. Values of this order were measured in two fibres under current clamp from the membrane potential response to current pulses. There is a large uncertainty in such a measurement, however, because of stray

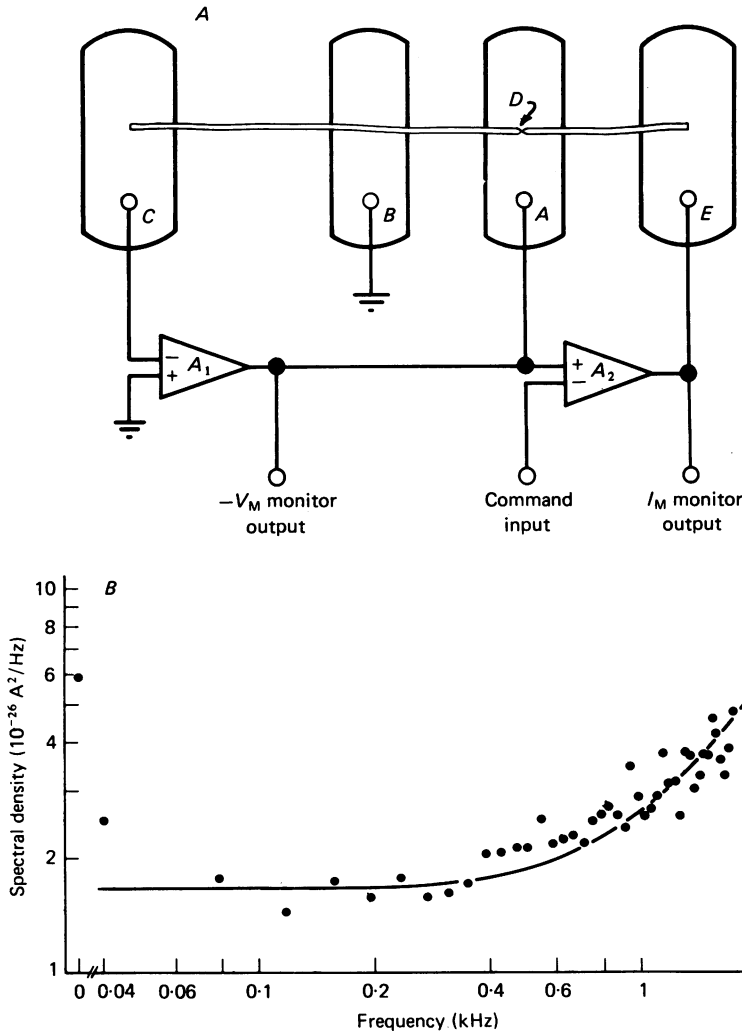

Fig. 1. *A*, simplified schematic diagram of the preparation and voltage clamp. The fibre is laid across insulating partitions separating the four pools *C*, *B*, *A* and *E*. The node is in pool *A*; pools *A* and *B* contain Ringer solution, while *C* and *E* contain 'end pool' solution (see text). Electrical contact with the pools is made through 1 M-KCl salt bridges to Ag-AgCl electrodes. The current in pool *C*, and therefore the voltage at the point *D* inside the nodal membrane is forced to be zero by the action of amplifier A_1. Amplifier A_2 acts to make the voltage at *A*, which is the transmembrane potential, equal to the command. The current flowing into the node is monitored by the voltage drop in the internodal axoplasm resistance R_{ED}. The length of the *ED* fibre segment is typically 800 μm, and the *CD* segment, about 1500 μm. *B*, spectral density of the membrane current noise at the holding potential E = −75 mV in node 13. The smooth curve shows the spectrum of the thermal noise calculated from the measured preparation resistances using eqns. (11)–(15) of Conti *et al.* 1976*a*. The only free parameter in the calculation was the membrane capacitance *C*, which was set equal to 6 pF. This value is larger than the initial capacitance values given in Table 1 and reflects the unusually large increase of capacitance with time during this experiment (see text).

capacitances and the limited band width of the potentiometric feed-back loop. This value is similar to a previous estimate for the node of Ranvier (Drouin & Neumcke, 1974).

To characterize adequately each fibre preparation for fluctuation experiments, four resistances were measured. The internodal resistances R_{DE} and R_{CD}, the seal resistance R_{BC} and the resting membrane resistance R_M had to be known because they determine the magnitude of the thermal noise background in the current fluctuations. R_{ED} also serves as the current-measuring resistance, and determines the scaling of the current monitor signal. As in van den Berg (1978) the resistances

TABLE 1. Basic parameters of the fibres used in this work. Nodes 12–19 are from *Rana temporaria*, while 21–43 are from northern *Rana pipiens* frogs. The seal resistance R_{BC}, internodal resistances R_{CD} and R_{ED} and the resting membrane resistance R_M are given in megohms. The initial, apparent nodal capacitance C is given in pF and the approximate fibre diameter in μm. The absolute sodium current reversal potential E_{Na} is given in mV; the peak sodium current I_p during depolarizations to -5 mV in nA; the single channel conductance γ near 0 mV in pS; and the total number of sodium channels N in thousands. Error bounds on the mean values are standard deviations

Node	R_{BC}	R_{CD}	R_{ED}	R_M	C	diam.	E_{Na}	I_p	γ	N
12	24	52	32	100	—	—	46	6·3	6·4	30
13	19	73	47	49	—	12	45	6·6	7·6	40
14	20	49	31	96	1·9	14	65	4·8	5·6	—
19	20	54	38	110	2·7	—	54	7·7	5·8	43
21	11	54	20	35	3·0	—	55	8·0	5·8	—
22	18	90	60	90	3·0	13	63	8·8	8·0	31
24	20	70	25	81	4·0	14	45	5·1	6·1	24
29	20	50	29	68	3·4	14	58	5·6	5·7	20
30	22	63	33	126	1·8	14·5	66	9·4	6·9	32
32	18	48	28	110	3·2	15·5	75	8·7	4·9	46
36	14	52	26	100	2·3	—	68	5·6	6·4	24
38	27	76	37	126	2·2	12	64	6·8	7·3	22
39	21	24	10·5	45	3·8	17	60	10·9	6·5	41
43	13	40	21	100	3·3	16	58	6·4	6·9	21
							59 ± 9 mV		$6{\cdot}4 \pm 0{\cdot}9$ pS	

were computed from electrical measurements on the intact nerve fibres; however, the technique used here did not require the additional F pool in the chamber. One set of measurements was of the current in pool C that was induced by perturbations in the voltage at A, B and E. Another kind of measurement was the ratio of the currents at C and E from a nodal action potential. From the four measurements the values of the four resistances were determined. The resistances and other properties of each preparation are given in Table 1. Fig. 1*B* shows a comparison of the spectrum of the current noise at the resting potential in one fibre with the prediction for the background noise using the measured resistance values.

The delivery of the command pulses and the recording of the responses were both controlled by a computer (Fig. 2). A programmable stimulator provided both the pulse sequence to the voltage clamp and the sample commands to the analogue-to-digital converter. The use of common timing circuitry for the stimulus and analogue-to-digital (A–D) conversion was essential for the ensemble fluctuation experiments. The apparatus used for these experiments showed fluctuations in the relative timing of stimulus and sampling of 20 ns. These fluctuations were measured by substituting a passive electrical network for the nerve preparation and observing the fluctuations in the recorded response during rapid current transients. Both the stimulator and A–D converter communicated with the computer through a direct memory access interface. Optical isolators were used to isolate the voltage clamp from the computer.

The current monitor signal from the voltage clamp was filtered in most cases by a 5 kHz, 4 pole Bessel filter and sampled at 100 μs intervals. The 5 kHz band width was chosen as a

compromise between filtering the maximum amount of thermal noise (whose spectral density increases as f^2 above roughly 2 kHz) and preserving the fastest expected fluctuations due to the gating of sodium channels. A filter band width of 20 or 100 kHz and sample intervals of 20 or 10 μs were used for the instantaneous I–E measurements.

Procedure. After mounting the fibre, the internodal and seal resistances were measured several times and checked for repeatability. The membrane capacitance was also measured by comparing the membrane potential response to the response of a model circuit when hyperpolarizing current pulses were applied. The voltage-clamp offset was adjusted to give $h_\infty = 0{\cdot}7$,

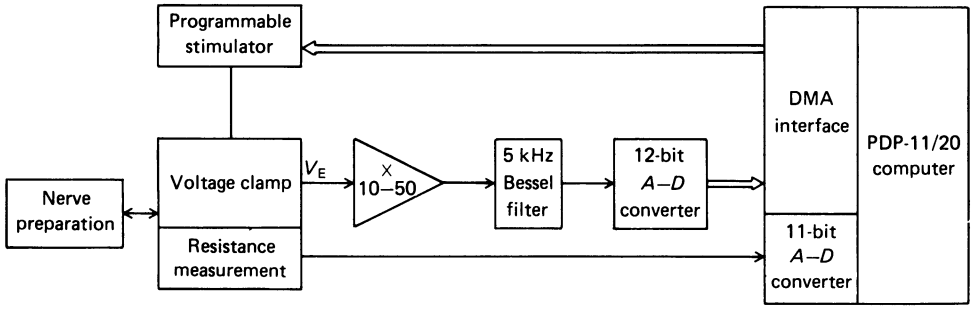

Fig. 2. Electronic configuration. A microprocessor-controlled stimulator (PSG-1, Page Digital Electronics, Monrovia, California) receives commands through a direct-memory-access (DMA) interface from the computer, and provides pulse sequences to the voltage clamp and sample commands to the analogue-to-digital (A–D) converter. The 12-bit A–D converter has a resolution of 2·5 mV which corresponded to 1–23 pA of membrane current depending on the internodal segment resistance R_{ED} and the amplifier gain chosen for the V_E signal. The resistance measurement involves the evaluation of transfer admittances in the preparation and is described in the Appendix.

as measured with 60 mV depolarizations; the holding potential established by this procedure was assumed to be -75 mV. Usually, records for activation and instantaneous I–V curves were then taken. The instantaneous I–V measurements employed a 1–2 ms activating pulse to $+45$ mV, chosen to be near E_{Na} in order to activate the sodium conductance with a minimum of ion-accumulation effects. A small depolarizing prepulse (-65 mV, 30 ms) was sometimes used, preceding the activating pulse, to reduce the peak current. In the early experiments (nodes 12–19) analogue leak subtraction was used, while later experiments used averaged and scaled responses to hyperpolarizations (to -115 or -135 mV, typically) for leak and capacitance current subtraction.

This preliminary data-taking typically occupied 20–30 min. The remaining 0·5–2 hr of each experiment consisted of fluctuation analysis runs, interspersed with checks of the holding potential, E_{Na} and the resistances. Immediately before and after each run, the responses to 16 hyperpolarizations to -115 mV were averaged; these were used to subtract the leak and capacitance currents from the mean current records. During the runs, pulse pairs consisting of a 50 ms prepulse and a 20 ms test pulse were applied at regular intervals in the range 300–600 ms. To avoid possible errors from short-term, use-dependent effects on the sodium current, the first 16 or more current records in each run were ignored. The responses from 100 to 1280 additional depolarizations were then recorded or processed on-line, as described below.

Computation of statistical parameters

The statistical parameters calculated from each ensemble of sodium current records were the mean and variance of the current at each sample point, and the non-stationary covariance function. The calculation and interpretation of the covariance will be considered in a later paper.

The variance was calculated from the residual fluctuations in each record after the mean time course of the current had been subtracted (Fig. 3). The mean time courses used for this subtraction

were local means, derived from groups of $n = 4$, 6 or 8 successive records. The use of local mean values prevented long-term drifts, which over the course of a run were occasionally as large as 10%, from contaminating the spontaneous, 1% fluctuations in the sodium current. It also allowed the computation and display of the statistical parameters to be performed during the experimental run. The disadvantage of using the local group mean time course rather than the ensemble time course for subtraction is that slightly more records are needed to obtain an equal scatter in the parameters. In effect, a fraction $1/n$ of the information in the records is lost in this process.

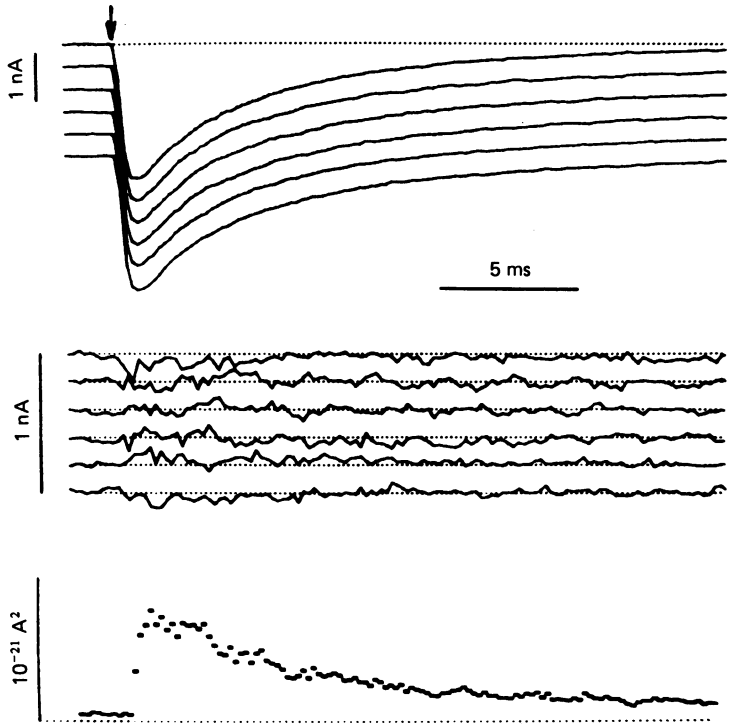

Fig. 3. Illustration of the ensemble variance calculation. *A*, six successive current records Y_{jk} from depolarizations to -5 mV, aligned at the start of the depolarizations (arrow). Linear leak subtraction was employed. *B*, residual current x_{jk} after subtracting the mean of a group of records. (Normally, groups consisted of four, six or eight records. Here, however, the mean of twelve records was used.) Note the larger deviations near the time of peak current. *C*, the variance at each sample point, computed from sixty-five groups of six records. Node 33.

The current records were processed in groups by the following procedure: Group mean (I_j) and variance (σ_j^2) estimates were calculated from the jth group of n records by evaluating

$$I_j(t) = \frac{1}{n} \sum_{k=1}^{n} y_{jk}(t)$$

$$\sigma_j^2(t) = \frac{1}{n-1} \sum_{k=1}^{n} x_{jk}^2(t) \qquad (1)$$

where y_{jk} is the k^{th} membrane current record and $x_{jk}(t) = y_{jk}(t) - I_j(t)$ is the deviation of each current sample from its group mean value. The calculations were done on-line and the quantities σ_j^2 and I_j were displayed so that the experimenter could reject those groups of records having noise spikes or unusually large variance values. At most, about 20% of the groups were rejected.

For the n_g groups that were not rejected, the group mean and variance estimates were accumulated to form grand averages $I(t)$ and $\sigma_j^2(t)$.

The variance estimate $\sigma^2(t)$ contains contributions from thermal noise in the voltage clamp and other undesired fluctuations, in addition to the sodium conductance fluctuations of interest. Assuming that the various fluctuations are uncorrelated, the variance σ_g^2 from the conductance fluctuations was taken to be

$$\sigma_g^2(t) = \sigma^2(t) - \sigma_{th}^2(t) \tag{2}$$

assuming that the other sources contribute negligibly to the variance. The calculation of σ_{th}^2, the variance from the thermal noise background, will be described below.

Interpretation of results

The instantaneous I–E measurements were fitted with the function

$$I(E) = I_s \frac{1-\exp\left[\beta_0(E_{Na}-E)\right]}{1+\exp\left[\beta_1(E_1-E)\right]} \tag{3}$$

where E_{Na} is the reversal potential and I_s is the saturation current at large E. The data from most fibres was well described with the values $\beta_0 = 0{\cdot}029\ \mathrm{mV}^{-1}$, $\beta_1 = 0{\cdot}025\ \mathrm{mV}^{-1}$, and $E_1 = 10$ mV. Eqn. (4) describes the saturation in I at large depolarizations better than the constant-field expression (Goldman, 1943) normally used for node of Ranvier sodium channels. Although it is similar to the I–E relationship for a non-saturating, two-barrier pore, the function is not intended to have any physical significance.

Values for the total number of channels N and the single-channel current i were estimated by fitting the functional relationship between the variance and mean current. The theory that was used is based on three assumptions about the sodium channels. First, they are assumed to exist only in either conducting or non-conducting states, with the probability p of being in the conducting state. Secondly, the gating of each channel is assumed to be statistically independent of the state of other channels. And, thirdly, the population of channels is assumed to be homogeneous. Under these assumptions the variance σ_g^2 and mean current I are related by (Ehrenstein, Lecar & Nossal, 1970; Begenisich & Stevens, 1975).

$$\begin{aligned} I &= Npi \\ \sigma_g^2 &= N\,p(1-p)i^2 \end{aligned} \tag{4}$$

The functional p embodies the average gating behaviour of the channels and depends on time and the history of the membrane potential. Eliminating p from the equations gives the expression that was fitted to the experimental data to yield values for i and N,

$$\sigma_g^2 = iI - \frac{1}{N} I^2 \tag{5}$$

Single-channel conductances γ were calculated as the chord conductances $\gamma = I/(E-E_{Na})$ and were usually obtained at $E = -5$ mV.

Sources of excess fluctuations

The purpose of this section is to estimate the possible errors arising from various instrumental and computational sources of fluctuations. The main instrumental source, the thermal noise in the voltage-clamped preparation, makes a large contribution to the observed variance. Its magnitude was calculated for each set of current records. The other sources considered are long-term drifts, the analogue-to-digital conversion, and truncation error in the computer calculations.

Drift. One source of excess fluctuations is the gradual change in I_{Na} with time due to electrode drift and fibre run-down. Long term drifts in the experimental records were estimated by comparing the means of the first and last groups of n records, and the data was discarded if the relative drift $\delta I/I$ per record was larger than 10^{-3}. This criterion ensured that errors in the calculated single-channel current from long-term drift would be less than 5×10^{-14} A, and in the estimated number of channels N, at most 5%. Most sets of records had much smaller drifts

than this. An example of the long-term change in I_{Na} during a series of depolarizations is shown in Fig. 4, where the average relative decrease of current per record was $1{\cdot}1 \times 10^{-4}$.

Long-term changes in the internodal and seal resistances were small. Among the two or three measurements that were made during each experiment, an average decrease in R_{ED} of $4\% \pm 1{\cdot}2\%$ (S.D.) per hour was observed; R_{BC} and R_{CD} showed similar changes. The membrane capacitance C, however, increased considerably with time, often doubling in the course of a 2 h experiment. Such increases in C have been reported previously (Dodge & Frankenhaeuser, 1959; Hille, 1967). I_{Na} did not increase, however. Changes in C have no practical effect on the time

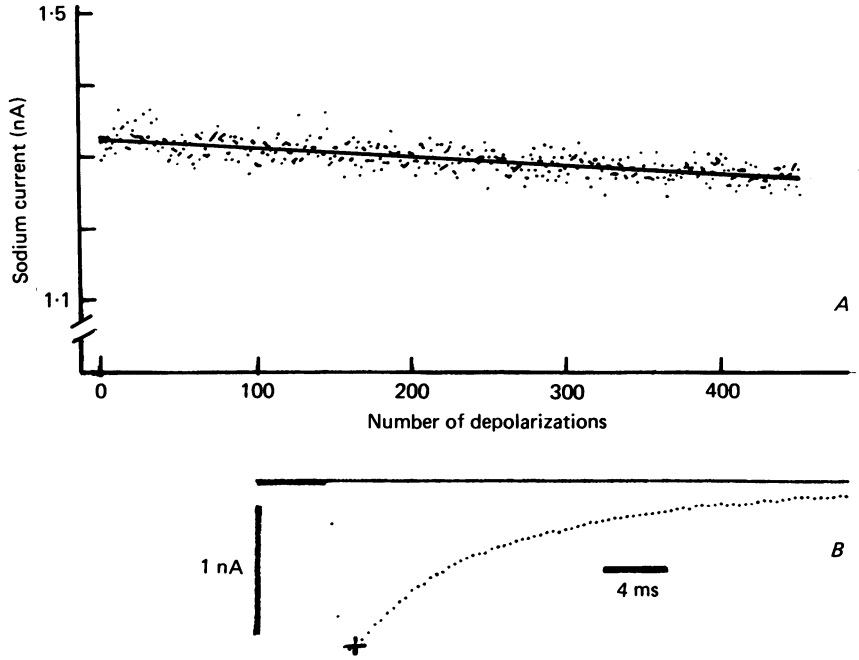

Fig. 4. *A*, long-term change in the current in node 33 recorded 1·6 ms after the start of each depolarization to −15 mV. *B*, typical current record, with the cursor indicating the current sample plotted in *A*. Responses to 450 depolarizations, delivered at 400 ms intervals and preceded by 50 ms prepulses to −65 mV, were filtered at 2 kHz and sampled at 0·4 ms intervals. The straight line has the slope −0·14 pA per pulse, or about −0·01 % per pulse.

course of either the mean current or the time-dependent part of the variance. However, the constant component of the background variance (b in eqn. (6)) will be shown to depend on C. Because C was measured at most only twice during each experiment, the prediction for the constant background component was too small in some cases and was usually left as a free parameter in fitting theoretical curves to the variance data.

Quantizing noise and truncation errors. At the lowest gain setting used in these experiments, the *A–D* converter quantizing interval corresponded to at most 12 pA. Since typical variance values were in the order of 2×10^{-21} A^2, corresponding to r.m.s. fluctuations of about 50 pA, quantizing noise contributed an error of at most a few percent to the variance estimates.

The on-line calculation of the variance and autocovariance functions required the speed of integer arithmetic operations, rather than the slower floating-point operations, in the computer. The calculation and subtraction of the mean preserved the full precision of the digitized current samples. In some experiments a division step preceding the squaring step in calculating the variance truncated 1–2 of the least significant bits, however. This introduced a truncation error of about 10% in some of the variance estimates. An appropriate correction was applied

to these estimates, calculated assuming a normal probability distribution for the ensemble fluctuations.

Estimation of the thermal noise background. Conti *et al.* (1976*a*) have shown that the instrumental contribution to the current noise spectral density depends on the full membrane admittance, including the instantaneous ionic conductance and the effects of the voltage-dependence of the conductances. The part of the thermal noise variance that involves the total instantaneous conductance of the membrane G_m can be written in the form

$$\sigma_{th}^2 = a_0 + b + a_1 G_m + a_2 G_m^2 \tag{6}$$

For these fibres a_1 was in the range of 1·1 (node 39) to 4·1 (node 21) $\times 10^{-24}$ A²/nS, while a_2 was 0·004 to 0·043 $\times 10^{-24}$ A²/(nS)².

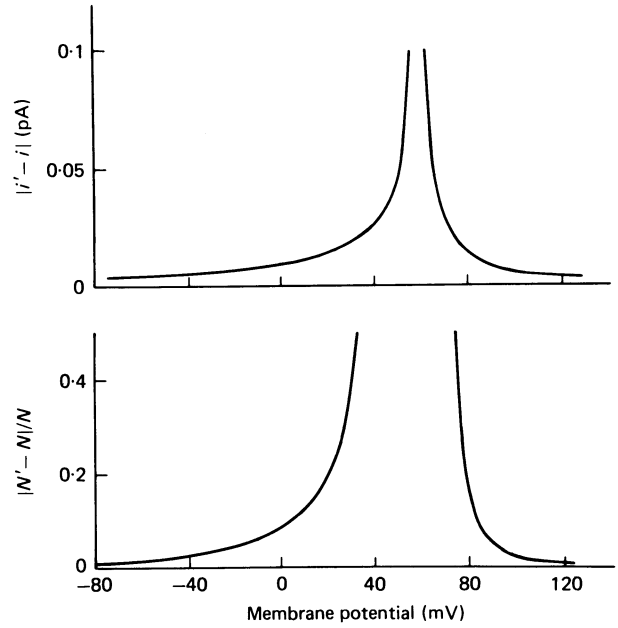

Fig. 5. Expected magnitude of errors in the apparent single-channel current i' and number of channel N' due to imperfect estimation of the thermal noise background. Errors were calculated from eqns. (5) and (6) with the coefficients a_1 and a_2 assumed to be in error by 20%. (The values from node 30, 1·9 $\times 10^{-24}$ A²/nS and 0·02 $\times 10^{-24}$ A²/(nS)², were used for a_1 and a_2.) The errors are largest near E_{Na}, where the current fluctuations from channels vanish. The asymmetry in the curves arises from the rectification of channels.

An additional component σ_a^2 of background fluctuations, not included in eqn. (6), arises from the voltage sensitivity of the sodium conductance as the clamp imposes voltage fluctuations on the membrane. The voltage fluctuations, which arise from the noisy estimate of membrane potential that is provided to the clamp amplifier, have a spectral density $S_V = 4k_BT\ R_{CD}(1 + R_{CD}/R_{BC})$. The resulting current variance component is largest at potentials where the activation of the conductance is most voltage dependent, and increases with increasing relaxation rate λ of the sodium conductance:

$$\sigma_a^2 \cong S_V \lambda \left(\frac{\partial p}{\partial V}\right)^2 I^2 \tag{7}$$

From the effect of small voltage displacements that were made during depolarizing pulses in one experiment, λ was measured to be about 5 $\times 10^3$ sec^{-1} at $E = -35$ mV, which is the potential

at which $\partial p/\partial V$ assumes its maximum value of about 100 V^{-1}. (The Hodgkin–Huxley theory predicts that $\lambda = \tau_m^{-1}$, which is, surprisingly, only about one third of the value that was observed.)

These values make $\sigma_a^2 \cong 5 \times 10^{-5} I^2$, which is of the same order as the coefficient $1/N$ of the second term in eqn. (5). An error of this size would therefore make an estimate of N entirely meaningless. However, the quantity $(\partial p/\partial V)^2$ has a large voltage dependence, such that the error becomes negligible for $E > -20$ mV. Because this error in the variance is proportional to the square of the current, it affects only the second term of (5) and is not expected to influence estimates of i, which come from the first term, at any potential.

Effect of errors in the estimation of the background. The thermal noise variance (6) depends quadratically on the membrane current, as does the variance from channel gating according to the two-state theory (5). It is therefore important to place bounds on the errors in the values of i and N estimated from (5) due to errors in the background estimation. The relative errors in the coefficients may have been as large as 20% since determinations of the resistances, especially the ratio of R_{BD}/R_{OD} (see Appendix), probably had errors of 5–10%. Errors of this magnitude would typically have caused the estimate of γ at -5 mV to be in error by 0·2 pS, and the value of N by 8%. Fig. 5 shows the expected size of the errors as a function of the potential during the depolarizations. The curves were calculated using the coefficients a_1 and a_2 for node 30, which gave the median values among the nodes in Table 1; the errors in the coefficients were assumed to be 20%. As can be seen in the Figure, estimates for N were more sensitive to background errors than γ values. The major source of error in γ values probably was the error in the estimation of the current-measuring resistance R_{BD}, rather than background errors.

RESULTS

The primary result presented in this section is the close correspondence between the predictions of the two conductance-state (open-closed) theory for channel gating and the observed relationship between the mean and variance of the sodium currents. On the basis of the theory, values are then obtained for the single-channel currents i and the number of channels N. Also, the first experimental determination of the fraction of channels open at the time of the peak current will be presented, and compared with bounds from other sources. Before discussing these main results, however, three experiments will be described that identify the corrected variance σ_g^2 with the spontaneous fluctuations in sodium conductance, as will be assumed in the theory.

The fluctuations are related to the sodium current

Fig. 6 shows the time course of the mean current, the total ensemble variance and the predicted thermal noise contribution to the variance from depolarizations to -15 mV. The time course of the variance is seen to be similar to that of the mean current, but has a peak that is less sharp. The peak variance value is about 2·4 $\times 10^{-21}$ A^2, corresponding to a standard deviation of 49 pA, or 0·9% of the peak mean current value. The predicted thermal noise background σ_{th}^2 accounts for 30% of the total variance at the peak. As in all noise analysis experiments, the source of the remaining variance σ_g^2, which is to be studied, must be identified as rigorously as possible.

To this end, two kinds of control experiments were performed, in which the sodium current was eliminated and the residual fluctuations were studied. Fig. 7*A* shows the variance and background prediction for a set of depolarizations from the first kind of experiment, where the sodium current had been blocked by 200 nM-

TTX. The absence of a detectable change ($< 2 \times 10^{-23}$ A^2) in the variance on depolarizing the membrane suggests that the fluctuations in the leakage current and residual potassium current are small. If the total mean current of 1·3 nA were carried by spontaneously gated channels, their single-channel current would be 10^{-14} A or smaller.

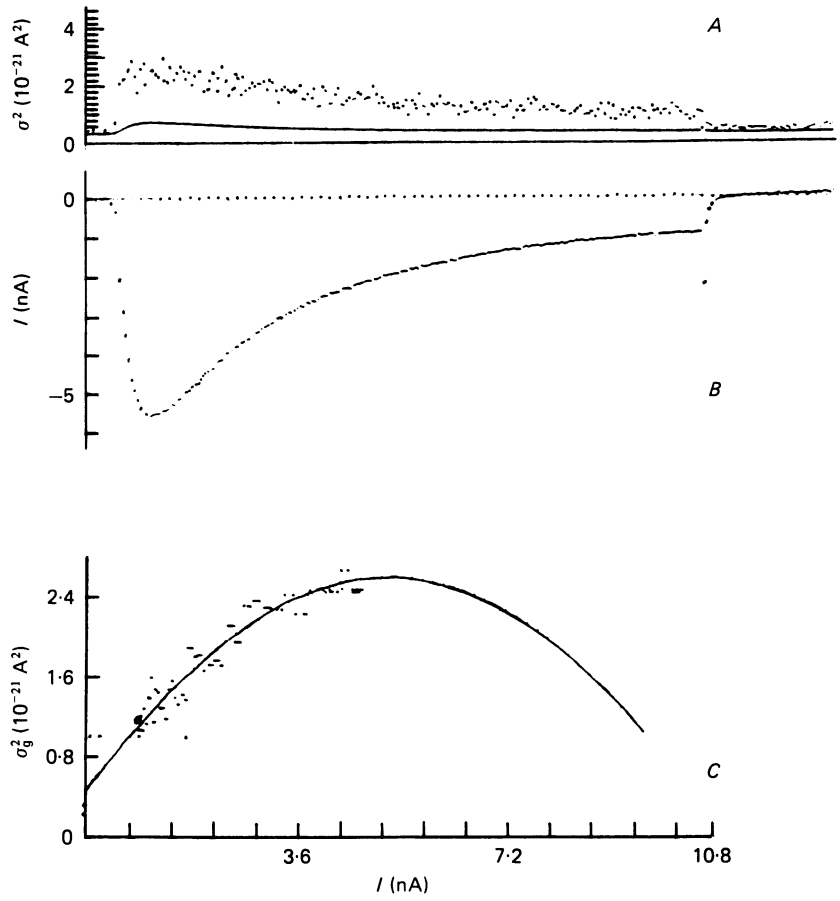

Fig. 6. Variance and mean sodium current from thirty-two groups of four 20 ms depolarizations to −15 mV after 50 ms prepulses to −105 mV. *A*, variance calculated at each sample point. The continuous curve is the thermal noise contribution to the variance calculated from eqn. (7). *B*, time course of the mean current from a group of four depolarizations. *C*, scatter plot of the variance and mean values. Each plotted point is the average of four sample points. The continuous curve is drawn from eqn. (5) with $i = -0{\cdot}55$ pA and $N = 20{,}400$. Node 43. In this and all succeeding variance-mean plots the scales are normalized such that an initial slope of unity corresponds to a chord conductance of 5 pS.

Results from the second kind of experiment are shown in Fig. 7*B*. Depolarizations were made to near the sodium current reversal potential E_{Na}, where the current fluctuations due to spontaneous channel gating vanish. However, at E_{Na} the sodium conductance does not vanish and the thermal motion of ions through the open sodium channels still takes place, so that the conductance-dependent thermal noise

variance (eqn. (7)) is present. The prediction for the thermal noise variance σ^2_{th} shown in Fig. 7*B* was calculated in the usual way, except that the time course of the membrane conductance was obtained by subtracting current records from depolarizations near E_{Na} but differing by 20 mV. (This subtraction step was necessary because of the distorted current time course seen near E_{Na} in the node of Ranvier preparation.) The prediction accounts for all but 14 % of the observed variance at

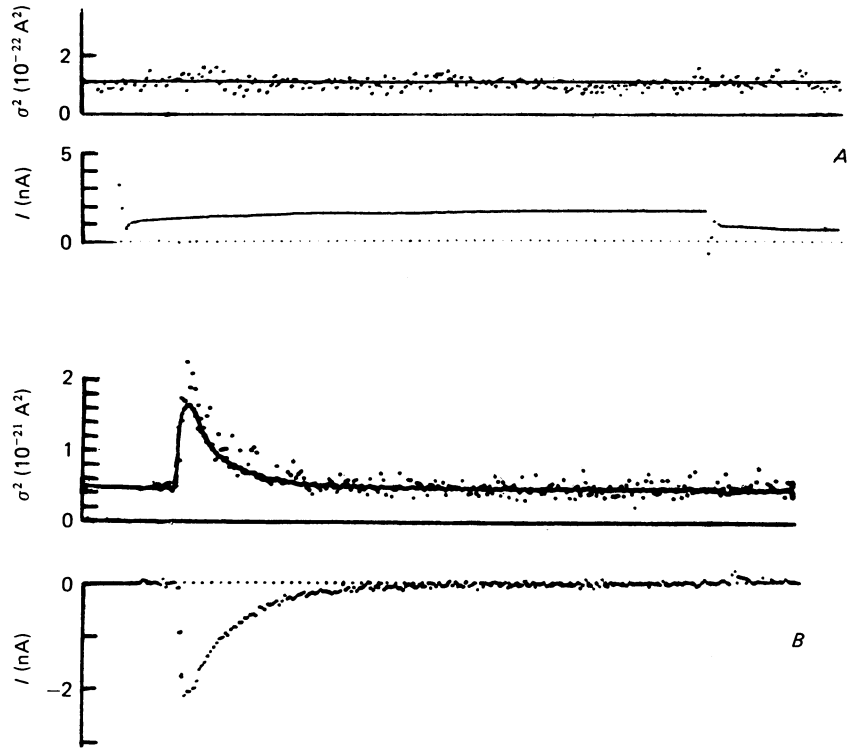

Fig. 7. Variance and mean current during 20 ms depolarizations in the absence of sodium current. *A*, with 200 nM-TTX applied to node 27. Upper trace is the total variance, which shows little deviation from the background level indicated by the line. The mean current (lower trace) with no leak or capacitance subtraction shows no sodium current. *B*, from depolarizations to + 50 mV (chosen to be near $E_{Na} \simeq 68$ mV) in node 36, which had a relatively high background noise level. Upper trace is the total variance; continuous curve is the predicted thermal noise background. The lower trace is the difference of two sets of current records, obtained at + 50 and + 70 mV. This difference was used to estimate the membrane conductance.

the peak. The correspondence between the observed variance and the prediction is a strong test of the adequacy of the thermal noise background calculation. This experiment is also a check for excess current fluctuations due to drift or noise in the voltage imposed on the membrane. These two experiments together show that nearly all of the difference between the total variance and the thermal noise estimate represents fluctuations in the sodium current.

A third test for unaccounted-for sources of fluctuations makes use of the different spectral properties of the expected sodium conductance fluctuations and the instru-

mentation noise. The temporal structure of the fluctuations can be described by the covariance function $c(t_0+\tau,t_0) = < x(t_0+\tau) \times (t_0) >$ which describes the correlation between values of the fluctuations at different times. When $\tau = 0$, the covariance is equal to the variance $\sigma_g^2(t_0)$. The part of c that arises from gating fluctuations is expected to be slowly varying in τ, with components having time constants in the order of τ_m or longer. The instrumental noise, on the other hand, contributes a narrow peak, centred on $\tau = 0$, corresponding to the autocorrelation of the low-pass filter response.

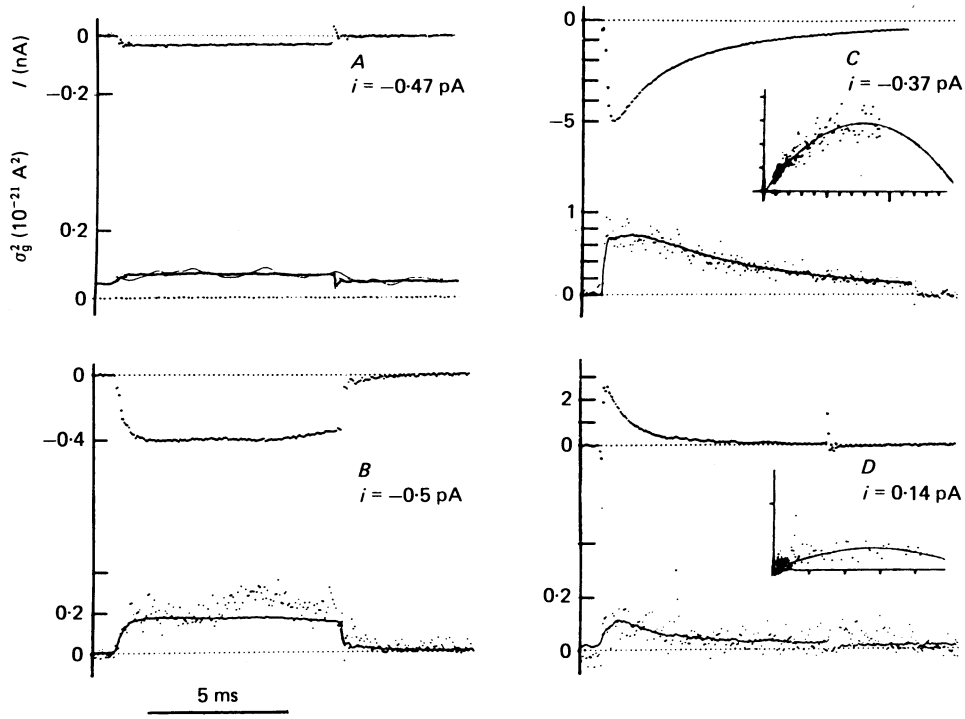

Fig. 8. Comparison of the time course of the mean current (upper traces) from 0 ms depolarizations to *A*, −55; *B*, −45; *C*, −5; *D*, +125 mV. The variance in *A* was smoothed with a gaussian function of 2 ms width. The smooth curve superimposed on the variance is the prediction of eqn. (5) from the time course of the mean current, with an arbitrary constant σ_0^2 added for the best fit. $N = 24{,}000$ in each case; the value of i is given for each pair of traces. The insets in *C* and *D* show the variance (ordinate) as a function of the mean current (abscissa); each small division corresponds to $2{\cdot}5 \times 10^{-22}$ A² and 0·5 nA, respectively, in *C*, and 0·6 nA and $3{\cdot}2 \times 10^{-22}$ A² in *D*. The curves are drawn with the same parameters as in the fits to the time course. Node 24.

The component of the variance arising from gating fluctuations can be independently estimated by extrapolating the slowly-varying component of the autocovariance over the region $\tau = 0 \pm 100\ \mu$s where the instrumental noise makes its contribution. Estimates of σ_g^2 from node 19 were made in this way, and they agreed with the directly-calculated values of σ_g^2 within 11 %. The fluctuations giving rise to σ_g^2 therefore also seem to have the spectral properties expected for sodium conductance fluctuations.

The two-conductance-state theory

At this point the corrected variance σ_g^2 has been identified with spontaneous fluctuations in the sodium conductance. As in most studies of membrane current fluctuations, the assumption is now made that these fluctuations arise from the statistically independent conductance fluctuations of many individual channels. When the corrected variance during a depolarization is plotted as a function of the mean current I (time being the independent parameter) as in Fig. 6*B*, the relationship is well fitted by a quadratic function. The variance is seen to increase with the mean current at low current levels, but to level off at high current levels. This kind of behaviour is predicted by the two-state theory for channel gating that gives rise to eqns. (4) and (5).

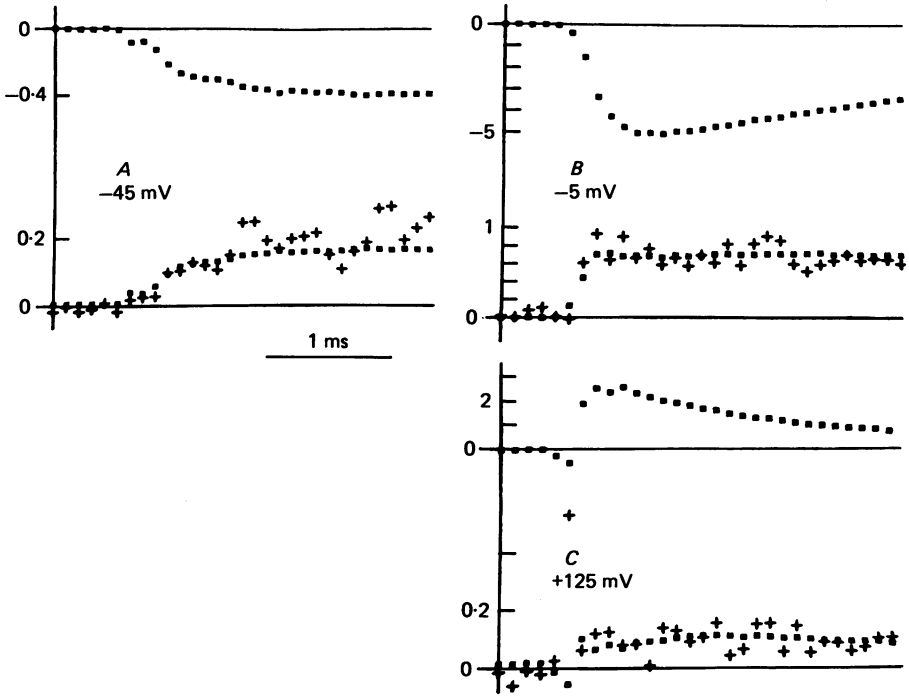

Fig. 9. Data of Fig. 8 plotted on an expanded time scale to show the rising phases of the mean current (upper) and variance (crosses, lower) time courses. The squares in the lower trace of each pair are the fits using eqn. (5) with the same parameters as in Fig. 8. Node 24.

In Fig. 8 and 9 the time course of σ_g^2 at several depolarizations is compared with the mean current time course. Superimposed on the variance points are the theoretical time courses for the variance derived from the mean current using eqn. (5). A fixed value of 24,000 was used for the parameter N, while values for i were chosen for a best fit at each voltage. A second free parameter in the fits was a small constant variance term σ_0^2 to compensate for errors in the steady-state background estimation. When the data is plotted on an expanded time scale (Fig. 9) the time course of the variance and the prediction are seen to match well during the activation phase. This

suggests that no change in the average single-channel conductance occurs during activation, which is a premise of the two-state theory. The agreement during the inactivation phase (Fig. 8) is also good, and supports the conclusion of Conti *et al.* (1976*b*) that inactivation is an all-or-none process.

Two predictions of the two-state theory can be tested by experiments. First, the value of N determined by fits to eqn. (5) should be a constant for each node of Ranvier, independent of the size of the depolarizations. This prediction was tested by constraining the value of N in the fits of Figs. 8 and 9. It should be noted, however, that the choice of N altered the shape of the predicted curves only at -5 and $+125$ mV depolarizations, where p became large.

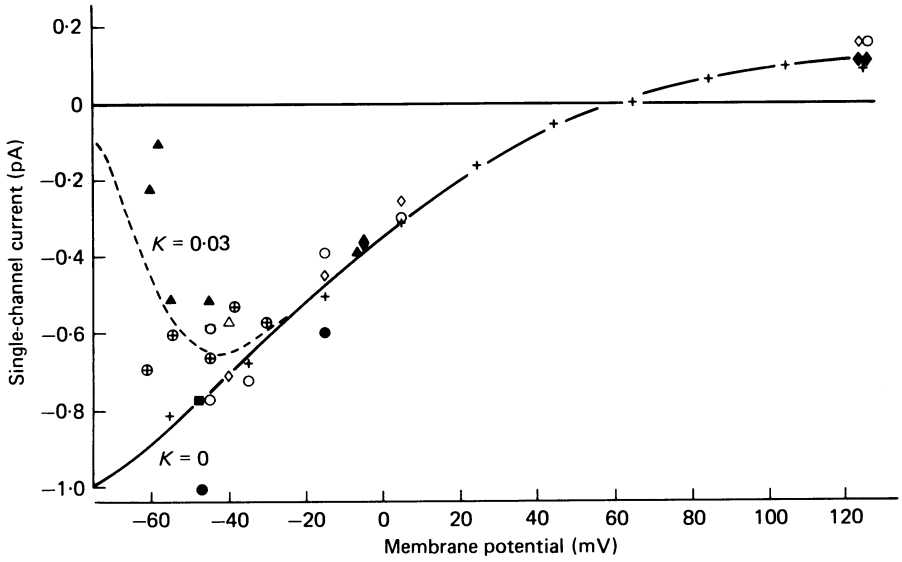

Fig. 10. Comparison of instantaneous current–voltage relation (crosses) with single-channel current values i obtained from fluctuation analysis. Open symbols are from *Rana temporaria*, nodes ○12, △13, ◇14; closed symbols from *Rana pipiens*, nodes ■21, ●22, ▲24, ◆29. The instantaneous I–V relation from node 39(+) was scaled by a factor of 1/26,000 to superimpose on the single-channel currents. It was obtained by stepping to the indicated potential after a 30 ms prepulse to -105 mV and a 1 ms conditioning pulse to $+45$ mV. The points are single-channel currents values calculated from the data of Conti *et al.* (1976*b*). The dashed curve is the prediction of the Hill & Chen theory with $\kappa = 0{\cdot}03$.

The second prediction of the two-state theory is that the instantaneous current–voltage relationship for the whole membrane should have the same form as the single-channel current–voltage relationship. The instantaneous currents for node 39, scaled by the factor 1/26,000, are plotted in Fig. 10 along with a curve drawn according to the fitting function (3).

Also plotted in the Figure are values of the single-channel current i obtained from fluctuation analysis of step depolarizations as in Figs. 8 and 9. In the two-state theory the instantaneous current values should be proportional to i, with the number of channels open at the beginning of the test pulse ($Np \cong 26{,}000$ in this

case) being independent of the test pulse potential. The voltage dependences of the two different current measurements do agree well over the range of -45 to $+125$ mV. Over this potential range the peak mean currents during the depolarizations in the fluctuation experiments ranged from about 10^{-10} A at -45 mV to 10^{-8} A at -15 mV. At smaller depolarizations the small currents yield variances σ_g^2 that are small compared to the steady background variance and are therefore difficult to estimate. Values of i were not estimated near E_{Na} because errors in σ_{th}^2 make large contributions there (see Fig. 5). The most reliable i values were obtained in the range -40 to $+10$ mV and at $+125$ mV. At these potentials a good agreement is seen between the instantaneous current–voltage relationship (a 'macroscopic' membrane property) and the single-channel current estimates determined by an entirely different method (fluctuations among current records).

TABLE 2. Single channel conductance γ and peak fraction of channels open p_{max} at $+125$ mV. Depolarizations were preceded by 50 ms prepulses to -105 mV

	γ (pS) at Δf (kHz)			
Node	2	5	10	p_{max}
22	1·6	—	—	0·94
24	—	2·0	2·9	0·93
29	—	1·9	—	0·84

The agreement shows that an average channel open at the time of the voltage-jump in the instantaneous current experiment has the same I–E relationship as the average channel opened by a steady depolarization at that test voltage. This would follow from channels being either open or closed, but would not necessarily be true if channels had more than one non-zero conductance level and if different conductance levels predominated at different potentials.

The single-channel conductance

Values for i and N were estimated for each node by curve-fitting, as in Fig. 8, from depolarizations to near $E = 0$. The resulting chord conductance values γ are given, along with estimates for N, in Table 1. The average γ value was $6{\cdot}4 \pm 0{\cdot}3$ pS (S.E. of mean) for all of the fibres. No difference in γ was seen between fibres from *Rana pipiens* and fibres from *Rana temporaria*.

Table 2 gives γ values from depolarizations to $+125$ mV; the chord conductances average 1·9 pS at this voltage. The small values do not indicate that the channels are in a state of lower conductance at this large depolarization, but instead reflect the considerable nonlinearity of the i–E relationship (Fig. 10). The Table also shows values for γ determined at this voltage using filter band widths of 2 and 10 kHz as well as the standard 5 kHz setting. The apparent increase at 10 kHz probably resulted from a poor correction for the thermal noise background, since the background variance increases by a factor greater than 4 when the band width is doubled from 5 to 10 kHz, and becomes much larger than the corrected variance σ_g^2. Another possible explanation for the increased γ at 10 kHz would be the presence of very fast gating fluctuations having a time constant of 30 μs or less. The variance from

these fluctuations would be substantially reduced by filtering at band widths of 5 kHz or less. The activation time constant τ_m is about 40 μs at this potential, so the existence of such rapid fluctuations would not be unreasonable. Their magnitude, however, is probably negligible, since activation is assumed to be nearly complete at +125 mV.

The activation process shows similarly rapid relaxations at depolarizations to less than −45 mV. Unlike the case at large depolarizations, however, the resulting rapid fluctuations probably constitute a large fraction of the total variance. Direct measurement of the variance at 10 kHz was unfortunately not possible because of the large background and the small currents. However, an observation of the gating kinetics suggests that the relaxations in this potential range are much faster than has been noted in the past.

I have studied the response of the sodium conductance when small (1–2 mV) perturbations in the membrane potential are made during depolarizations in the range of −50 to −35 mV. One result relevant to this work is that the relaxations induced by such perturbations were much faster than predicted by Hodgkin-Huxley kinetics. As Mauro *et al.* (1970) have shown, the component of the relaxation arising from the activation gating process is expected to have a single time constant τ_m. I found that a major component of the relaxations at −45 and −35 mV had time constants of about 200 and 90 μs respectively, which are about one third of the τ_m values.

The existence of fast relaxations at small depolarizations suggests that there is a fast, highly voltage-dependent gating step at these potentials that is normally masked by slower, rate-limiting steps in the activation process. This step would result in high-frequency fluctuations that may have been lost by filtering in these fluctuation experiments, causing i to be underestimated. Only half of the variance would be observed, for example, from fluctuations in a 30 μs gating process because of the 5 kHz filter band width. It is probable that the filtering of rapid fluctuations of this kind is at least partly responsible for the low values of i shown in Fig. 10 at small depolarizations.

Fraction of channels open at peak conductance

Within the framework of the two-state theory, the probability p_{max} that a channel is in the open state at the time of peak conductance at a given potential E can be calculated from experimentally determined quantities,

$$p_{max} = \frac{I_{max}(E)}{Ni(E)} \tag{8}$$

where $I_{max}(E)$ is the peak current during a steady depolarization to E. Values of p_{max} are given in Table 3 for depolarizations to near −5 mV and in Table 2 for depolarizations to +125 mV. In all cases the depolarizations were preceded by 50 ms prepulses to −105 mV to remove the resting inactivation. A majority (p_{max} = 0·6) of the channels appeared to be open at −5 mV, and nearly all (0·9) of them were open at the time of the peak current at +125 mV. The large p_{max} at +125 mV is a reflexion of the substantial decrease observed in the variance at the time of the peak current (Fig. 11).

Different theories of gating make different predictions and bounds for p_{max}. The Hodgkin-Huxley model for sodium channels, interpreted as describing independent, two-state channels, predicts p_{max} values of 0·58 and 0·83 for $E = -5$ and $+125$ mV. To obtain these values, I assumed m^3h kinetics and used the rate constants of Hille (1971*b*), scaled to 4° using the Q_{10} values of Frankenhaeuser & Moore (1963).

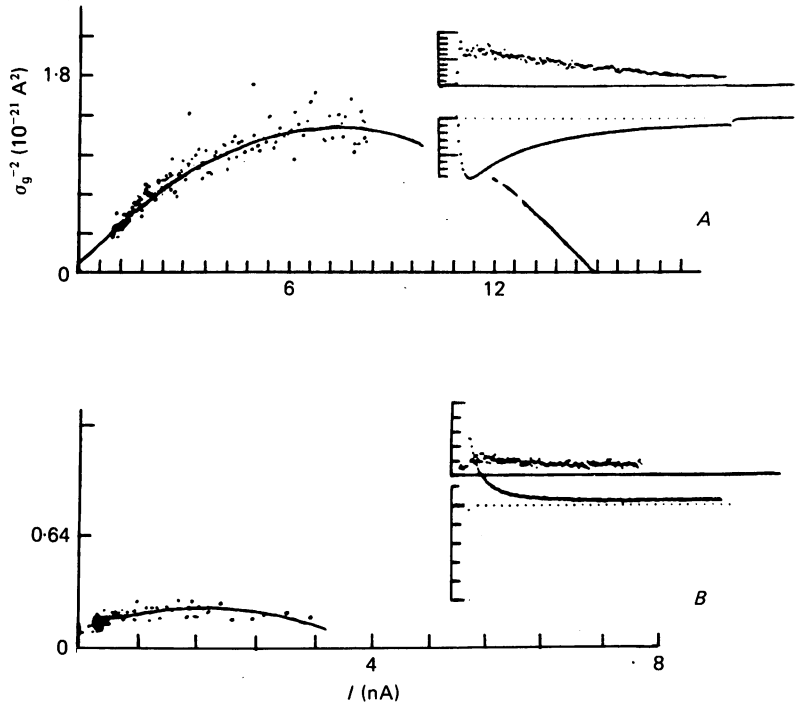

Fig. 11. Evidence for a majority of channels open. Variance-mean plots for depolarizations to *A*, −5 mV (node 19) and *B*, +125 mV (node 22) after −105 mV prepulses. Insets show the time course of the variance (upper trace) and mean current with scale factors of 2×10^{-22} A^2 and 1 nA per small division, respectively. The depolarizations lasted 20 ms. p_{max} values are *A*, 0·58 and *B*, 0·94.

Table 3 shows upper bounds for p_{max} predicted by two other theories of sodium channel gating. Current records obtained at −5 mV were fitted with sums of exponential functions, and these terms were assumed to have arisen from either an independent-inactivation or a coupled-inactivation gating process. In both cases a two-component inactivation time course was used (Chiu, 1977), and the steady state activation was assumed to be complete. In the independent-inactivation case, the bound on p_{max} was the peak value of the product of normalized activation and inactivation terms. The coupled-inactivation theory assumed, for simplicity, that only activated channels could inactivate, so p_{max} was the peak value of a convolution of the two processes. The experimental p_{max} always fell below these upper bounds, so that no discrimination between these two theories was possible.

Both of these theories predicted bounds greater than 0·98 for p_{max} at +125 mV

because the activation is extremely fast relative to inactivation at that potential. The observed p_{max} value of 0·90 (see Table 2) indicates that activation is essentially complete in this case. It should be noted that the possibility of systematic errors in the N and therefore in the p_{max} estimates could cause the values to be in error by as much as 10%. It is possible that nearly every channel is open at the peak of conductance at +125 mV.

TABLE 3. Peak fraction of channels open p_{max} at −5 mV. Values are from depolarizations preceded by 50 ms prepulses to −105 mV. Upper bounds are computed from fits to the kinetics of the currents, assuming activation is maximal. The average p_{max} value is given ± S.D

		Upper bounds	
Node	p_{max}	indep.	coupled
19	0·58	0·80	0·89
22	0·48	0·76	0·90
24	0·65	0·78	0·89
38	0·68	0·76	0·90
39	0·55	0·78	0·92
	0·59 ± 0·1	0·77	0·90

DISCUSSION

The relationship between the mean current and the corrected variance has been used to calculate single-channel currents and the number of channels in each fibre. The first question to be addressed in this section is, what are the sources of error in these values? In the Methods section, I showed that errors in the background variance estimation have varying effects on the apparent i and N values, depending on the membrane potential. Errors could have also come from a transport noise component in the fluctuations and from excessive filtering. A second question to be addressed is, how incisive are the tests that have been presented for the two-conductance-state theory? Certain classes of multiple-state theories would not have been discriminated from the two-state theory on the basis of these experiments. Finally, the values of γ, N and p_{max} from this work will be compared with other values from the literature.

An upper bound on transport fluctuations

In principle it is difficult to distinguish between fluctuations in the transport of ions through open channels and fluctuations due to the opening and closing of channels. In the interpretation of these experiments, the variance contributed from transport fluctuations has been assumed to be zero. If it is in fact substantial, it may have caused the results to be in error. In nerve preparations where it has been measured, however, the variance from '$1/f$ noise' normally associated with transport fluctuations is usually seen to increase as the square of the mean current (Derksen, 1965; Poussart, 1971; Conti, DeFelice & Wanke, 1975; Fishman, Moore & Poussart, 1975; Conti *et al.* 1976*a*), while the variance as measured in the experiments reported here is seen to decrease at the highest current levels in large depolarizations (Fig. 11). An upper bound on the size of such a transport noise component in the observed variance can therefore be made by assuming that at the

instant of peak conductance during a large depolarization all of the channels are open ($p_{max} = 1$), so that all of the remaining fluctuations would be due to transport fluctuations. From the depolarization to +125 mV of Fig. 11*B*, the normalized variance from transport fluctuations

$$\sigma^2_{transport}/I^2 \cong 1{\cdot}1 \times 10^{-5}$$

corresponds to a conductance fluctuation of 0·3 %. The presence of transport fluctuations of this magnitude would cause N to be overestimated by about 7 %. There would be no effect on estimates of i, assuming that the transport noise variance increases as the square of the mean current, since i is derived from the linear term in the variance-mean relationship (6).

Low i values at small depolarizations

Like Conti *et al.* (1976*a*, *b*), I find small values for the apparent single-channel current at small depolarizations where the sodium conductance is less than 1 % of the maximum value. I used the constant field equation to determine values of i from their reported γ values; the resulting values, scaled to 5° assuming a Q_{10} of 1·3, are compared with the ones from my experiments in Fig. 10. The deviation of their i values from the instantaneous I–E relation at the smallest depolarizations is similar to but less pronounced than the deviation of my values. One explanation for the decrease of i at small depolarizations has already been considered. It is that high-frequency fluctuations from channel gating are being filtered, and are therefore not included in the observed variance. A second possibility is that voltage-dependent transitions among several conductances are allowing lower conductance levels to predominate at small depolarizations.

Channels with multiple open states. The equations for the mean current and variance (4) can be generalized for multiple levels of single-channel current,

$$I = N \sum_k p_k i_k$$

$$\sigma_I^2 = N \left[\sum_k p_k i_k^2 - \left(\sum_k p_k i_k\right)^2\right] \tag{8}$$

where p_k is the probability of a channel being in the kth state and i_k is the single-channel current in that state. Under conditions where the probability of a channel being in any of the conducting states is small, the second term in (8) vanishes and the apparent single-channel current

$$i' \equiv \frac{\sigma^2}{I} \simeq \frac{\sum_k p_k i_k^2}{\sum_k p_k i_k} \tag{9}$$

is determined by the initial slope of the variance-mean relationship. In the two-state case i' will be the single-channel current of eqn. (5) while for theories having more states the value of i' will lie between the largest and the smallest non-zero current values.

One test of multiple-state theories is the comparison of the voltage dependence of i' with the instantaneous I–V relationship. While the value of i' at a given voltage

depends on the values of the p_k at that voltage, in the instantaneous I–E experiment the values of the p_k will reflect the prepulse conditions before the step to the test voltage. An example of a multiple-state theory with voltage dependent p_k values is the Hill & Chen (1972) model modified to include an all-or-none inactivation process

$$i_k = \bar{i}\,\kappa^{(3-k)}$$

$$p_k = \binom{3}{1} h\, m^k (1-m)^{(3-k)} \tag{10}$$

where $\bar{i}$ is the maximum single-channel current, $0 \leqslant \kappa \leqslant 1$ is a parameter of the theory, and m and h are the usual Hodgkin-Huxley variables. This theory postulates four different single-channel current values, differing by factors of κ, that correspond

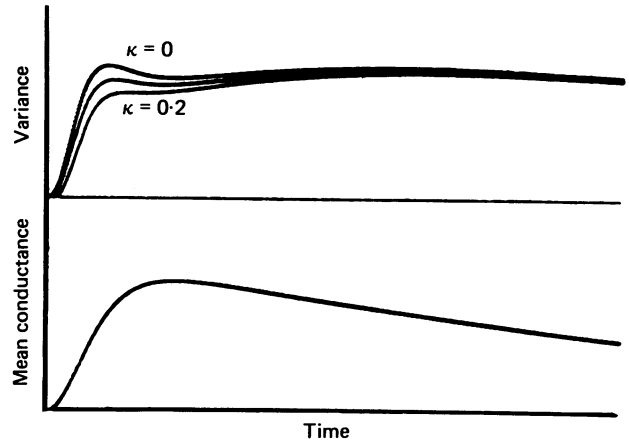

Fig. 12. Upper trace shows the time course of the variance predicted by the Hill & Chen theory for $k = 0$, 0·1 and 0·2. Lower trace shows the corresponding mean current time course, which is the same in each case. Calculated from m^3h kinetics with $\tau_h = 25\,\tau_m$; $m_\infty^3 = 0{\cdot}8$.

to different states of the activation gating process. The dashed line of Fig. 10 shows the voltage dependence of i', calculated from this theory using $\kappa = 0{\cdot}03$, while the solid curve represents $\kappa = 0$. The experimental values of i', which were obtained from curve fitting as in Fig. 8, can be compared with the theory because the assumption of eqn. (9) is valid at small depolarizations, where the differential predictions are largest. The Figure shows that if κ is non-zero, it must be very small.

A second test for multiple conductance states is to look for a time dependence in the apparent single-channel conductance. Even in the absence of a suitable voltage dependence of the transitions among the various conductance states, multiple-state effects would be apparent if the time courses of the p_k during a depolarizing pulse were sufficiently different. The Hill & Chen theory can, with different values of κ, predict different time courses for the variance while giving the same mean current time course. Unfortunately, κ must be relatively large to give an observable effect. Fig. 12 shows the variance time-course predictions of the theory for two conductance states ($\kappa = 0$) and for $\kappa = 0{\cdot}1$ and 0·2. Comparison with the experimental data of Figs. 8 and 9 shows that only for $\kappa \geqslant 0{\cdot}2$ would the time courses be sufficiently

different to distinguish between the theories. The voltage-dependence of i is a more sensitive test for the Hill & Chen theory.

There is a large class of gating theories that would appear, from the two tests described above, to behave like the two-state theory. Some multiple-state theories would not be discriminated because of scatter in the experimental data. For example, if two conductance levels differed by 10 % or less, or if the transition between two different conductance levels was both rapid ($< 0{\cdot}5$ ms) and relatively voltage-independent, the observed single-channel current i' would appear to reflect a single conductance level and the time course of the variance (as in Fig. 9) would be nearly the same. Still other theories make exactly the same predictions as the two-state theory. Channels having several kinetically distinct open states, all having the same conductance, or a mixture of channel types having identical gating properties but different conductances are two situations where a relationship between the variance and mean current exactly of the form of (5) obtains. Chandler & Meves (1970) and Armstrong & Bezanilla (1977) have invoked additional, kinetically distinct open states of the channel to explain their experimental results in squid axons. If such states also exist in the node of Ranvier sodium channel, the results of this work show that they probably have the same level of conductance. The simplest conclusion from these experimental results is that sodium channels have only one non-zero level of conductance. A lower conductance state might be present and could be partly responsible for the low apparent single-channel conductance at small depolarizations. I believe, however, that the low i values probably arise from the effect of the limited filter band width alone.

Single-channel properties

The single-channel conductance estimate of $6{\cdot}4 \pm 1$ pS obtained in this work is very close to the values 7·9 and 6·6 pS, in unmodified and modified channels respectively, from the experiments of Conti *et al.* (1976*b*) who also used the frog node of Ranvier preparation. Their experiments were performed at a higher temperature, 13 °C, rather than the range of 2–5 °C that I used. Assuming a Q_{10} value of 1·3 (Frankenhaeuser & Moore, 1963), the corresponding γ value from my work would be 8·3 pS at 13 °C. The agreement of γ values is remarkably good in view of the different assumptions underlying the two fluctuation analysis methods. The ensemble fluctuations analysis in my work assumed only that the relaxation times of the fluctuations were larger than about 30 μs, but required that the thermal noise variance be calculated and subtracted from the total variance. The experiments of Conti *et al.* on the other hand, did not require the thermal noise correction. They did, however, fit their power spectra to functions based on the Hodgkin–Huxley theory in order to separate the gating fluctuation component from the total variance. The value of γ reported here also falls in the range of values 1–8·6 pS obtained by various techniques in squid and frog nerve (summarized in Conti *et al.* 1976*b*).

I have found the number of channels N available for conduction in a node to be in the range 20,000–46,000. This is somewhat lower than the estimate of 10^5 given by Conti *et al.* The actual number of channels in a node may be larger than my estimate of N because ultra-slow inactivation may reduce the number of available

channels (Neumcke *et al.* 1979). In my work N was a parameter of the fits to the data; its determination did not require the assumption of a specific theory of gating.

I have also presented the first experimentally-determined values of p_{max}, which are near those predicted by the Hodgkin–Huxley theory. p_{max} could be measured because the ensemble analysis technique allowed the fluctuations to be observed at the maximum sodium conductance. The estimates for p_{max}, about 0·6 at -5 mV and 0·9 at $+125$ mV, are relatively sensitive to errors in the background correction and have an uncertainty of about 10 %.

Prediction of theshold fluctuations

From the properties of single sodium channels the expected size of threshold fluctuations in a node of Ranvier can now be calculated. Fluctuations in the response of single axons to threshold stimuli were discovered by Blair & Erlanger (1932) and Monnier & Jasper (1932), and were studied extensively by Verveen (1961). Verveen found that the probability p_{fire} of initiation of an action potential as a function of stimulus strength S was well fitted by the normal probability distribution. The relative spread of the fluctuations, $R = \sigma_s/S_0$, where S_0 is the threshold stimulus and σ_s is the standard deviation of the threshold, was independent of the stimulus duration, and had an average value of $1{\cdot}1 \pm 0{\cdot}5$ % for a frog phalangeal nerve preparation at 20 °C. Similarly-sized fluctuations, for which R was about 1·3 %, had previously been observed (Pecher, 1939; Erlanger, Blair & Schoepfle, 1941).

Lecar & Nossal (1971*a*, *b*) presented a theory for the threshold fluctuations in an isolated node and considered various possible sources of the fluctuations. They concluded that the predominant contribution to the fluctuations would come from the gating of sodium channels. Their value for the relative spread component R_σ from conductance fluctuations was about 4 %, considerably larger than the measured values. It now appears that this value was large mainly because their assumed value for the number of channels in a node, $N = 7500$, was an order of magnitude too small.

I have calculated R_σ using their equations, but with large values of N based on the measurements of γ and N in this work. Using $\gamma = 6{\cdot}4$ pS at 4 °C, increasing to 10 pS at 22 °C, I obtained values of R_σ near 1 %. The R_σ values were calculated from eqns. (36) of Lecar & Nossal (1971*a*) and (34) of the (1971*b*) paper, and were divided by $\sqrt{2}$ to correspond to Verveen's definition of R. Table 4 shows the two sets of nodal parameters that were used, and the resulting values of R_σ. One set is the parameters (Hille, 1971*b*) that Lecar and Nossal used in their original calculation, with only the number of channels N changed. The other set consists of the parameters for node 30 of this work. Although the $\bar{G}_{Na}$ value for this node was much smaller, the larger activation rate, determined from a perturbation experiment, resulted in a similar eigenvalue p_1 for the initial growth of the action potential and a similar value for R_σ.

Both Hille's standard node and node 30 were in fibres approximately 15 μm in diameter. The diameters of the fibres in the threshold fluctuation measurements are not known exactly, but Pecher estimated fibre diameters in the range 10–12 μm from his preparations, and Verveen (1961) gives an average internodal axon diameter

of 4 μm measured after fixation. The predicted value $R_\sigma \cong 1\%$ for 15 μm fibres therefore corresponds well to the experimental values of R which are near 1·2% for fibres about 10 μm in diameter.

TABLE 4. Nodal parameters and predictions for the relative threshold fluctuations R_σ. The notation of Lecar & Nossal (1979*a*, *b*) is used. The parameters for Node 30 were scaled to 22 °C using Q_{10} values of 1·8 for τ_m, 1·3 for G_{Na}, and 1·2 for G_o. The value for C was reduced to 1·5 from 1·8 pF to compensate for the increase of C observed in the isolated fibre.

Parameter	Symbol	Units	Hille, 22 °C	Node 30, 22 °C
Fibre diameter	d	μm	15	14·5
Resting potential	V_o	mV	−75	−75
Reversal potential	V_1	mV	48	66
Nodal capacitance	C	pF	1·5	1·5
Leak conductance	G_o	10^{-8} S	4·8	1·1
Maximum Na conductance	$G_{Na}h_\infty(V_o)$	10^{-7} S	6·3	2·2
Threshold potential	V_B	mV	−53·5	−50
Threshold G_{Na} activation	σ_B		0·0093	0·01
Steepness of activation at threshold	$d\sigma/dV$	V^{-1}	1·85	2·0
Activation rate (τ_m^{-1})	λ	10^4 sec^{-1}	1·0	3·3
Number of channels	N		10^5	32000
Positive eigenvalue	p_1	10^4 sec^{-1}	2·4	1·65
Relative spread (isolated node)	R_σ		0·8%	1·1%

The theory of Lecar & Nossal predicts the threshold fluctuations R_σ for an isolated node with no loading from the rest of the fibre. The experiments, on the other hand, measured the fluctuations for action potential initiation in intact fibres. A better, but more approximate, estimate of this relative spread R_{fiber} was made by adding an additional nodal conductance g' and capacitance C' to simulate the electrical loading of the stimulated node when the adjacent nodes are short-circuited. Because the characteristic rate p_1 of the action potential initiation is large, the shorted-nodes approximation is good since the effective impedance $1/p_1C$ of the adjacent nodes is smaller than the internodal resistance. Because of the increased conductance and capacitance, the threshold depolarization $V_B - V_0$ was increased by 6 mV. The resulting R_{fiber} values were slightly smaller, 0·7 and 0·9%, than the respective R_σ values.

From this analysis it can be seen that essentially all of the fluctuations in the firing threshold can be accounted for by sodium conductance fluctuations. Verveen's original hypothesis, that fluctuations in the firing threshold of axons reflect the underlying mechanism of excitability, formed the basis for the many studies that have been made of the current fluctuations in axon membranes. Now that the properties of sodium channels are better understood, it appears that Verveen was correct: the size of the fluctuations in axon excitability reflects the single-channel conductance and kinetics of sodium channels.

I thank Dr C. F. Stevens for helpful discussions and I am grateful for the privilege of working in his laboratory. I also thank Drs R. W. Tsien, R. Rogart, J. Strong for their comments on the manuscript and Drs F. Conti and B. Hille for raising the issue of voltage-driven gating fluctuations. This work was supported by U.S.P.H.S. grant no. 12962.

APPENDIX

The voltage-clamp circuitry

The voltage-clamp system incorporates several changes and enhancements over previous designs. Although it uses the chamber design of Hille (1971*a*) which requires longer internodal segments (and therefore has higher internodal resistances) than the design of Nonner (1969), it approaches the same level of performance in speed and background noise level. It also is the first myelinated nerve voltage clamp to incorporate series resistance compensation and a provision for measuring the internodal resistances in the intact preparation.

Feed-back amplifiers. Nonner demonstrated that by reducing the interelectrode capacitances and by tailoring the amplifier frequency response, a single-amplifier voltage clamp could achieve extremely rapid setting times. I chose to return to the two-amplifier design of Dodge & Frankenhauser's (1958) original voltage clamp (Fig. 13) because the control of A-pool voltage can be used to provide damping of the feed-back loop.

In this design, the potentiometric amplifier (A_1 in Figs. 1 and 13) is a transresistance amplifier, having a low input impedance because of the local feed-back provided by capacitor C_F. It senses a deviation in the voltage inside the node V_D by a current (rather than voltage) signal in the C pool and corrects the deviation by applying an appropriate voltage to the A pool. By making the C pool a low-impedance node through local feed-back, the stray capacitance to ground C_{BC} is in effect rendered invisible, and the pole in the open loop transfer function corresponding to the time constant $R_{BC}C_{BC}$ is shifted to a much higher frequency.

The transfer function of A_1 was chosen to complement the admittance Y_{DC}, measured as the current response at C to voltage changes in A after the nodal membrane had been destroyed. In measurements to 500 kHz on a 14 μm fibre, Y_{DC} showed a simple pole corresponding to a time constant of 1 μs, probably due to the myelin capacitance in the B pool. The transfer function of A_1 was therefore chosen to be that of an integrator, modified by a phase-lead network in the frequency range 160–800 kHz to move the effect of the pole in Y_{DC} to higher frequencies. The transresistance of A_1 falls from very large values at low frequencies to about $10^8\ \Omega$ at 100 kHz. Despite the extensive shielding, its usable gain is restricted above about 500 kHz by the residual coupling capacitance $C_{AC} \cong 2 \times 10^{-16}\ F$. The natural frequency of the potentiometric loop varies from about 50 kHz for a 12 μm fibre to about 200 kHz for a 17 μm fibre.

The voltage clamp amplifier A_2 is more conventional, but has a similar frequency response characteristic. Its gain falls with increasing frequency to a constant value of about 40 above 20 kHz. The natural frequency of the voltage clamp varies from 20 to 100 kHz for fibres 12 μm to 17 μm in diameter, and is limited by the residual capacitance $C_{EC} \cong 2 \times 10^{-17}$ F. The use of amplifiers with very high DC gains ensures that the clamped membrane potential, in the absence of effects like the attenuation artefact, will have no steady-state error. Accompanying this advantage, however, is the disadvantage of an increased overshoot in the response of the membrane potential to a step in the command voltage. A filter was therefore inserted to smooth the transitions in the command voltage and reduce the overshoot.

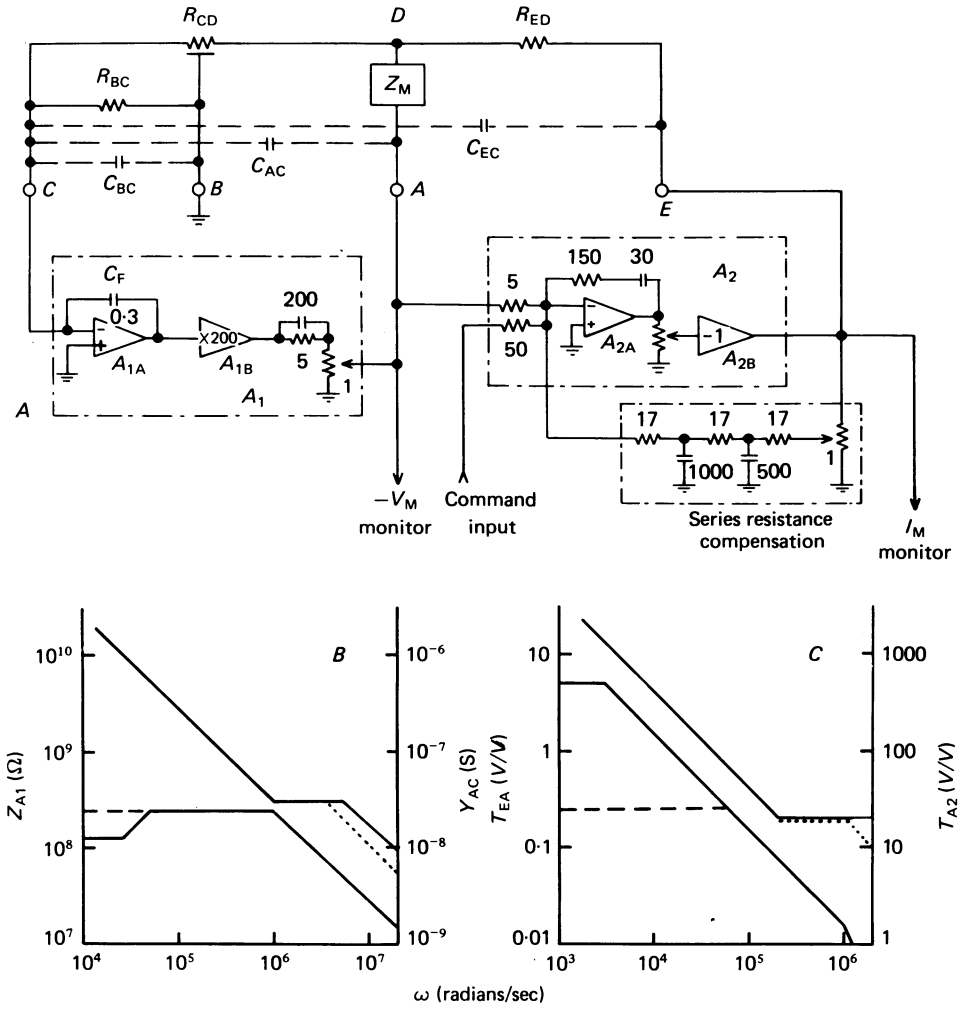

Fig. 13. *A*, schematic diagram of the model circuit for the preparation and of the voltage-clamp circuitry. Typical model parameters for a 15 μm fibre are R_{BC}, 20 MΩ; R_{CD}, 50 MΩ; R_{ED}, 30 MΩ. Z_M represents the nodal membrane. Stray capacitances at 100 kHz are approximately: C_{BC}, 3 pF (including amplifier input capacitance); C_{AC}, 2×10^{-16} F; C_{EC}, 2×10^{-17} F. The component values in the voltage-clamp amplifiers are given in kilohms and picoforads. A_{1A} is an operational amplifier built with discrete components using an NDF9401 (National Semiconductor) dual field-effect transistor in the first stage. It has a voltage noise spectral density of 11 nV/Hz$^{\frac{1}{2}}$ above 10 Hz and a band width of 6 MHz at the closed-loop gain of 10. A_{1B} also consists of discrete components, and has a band width of 2 MHz. A_{2A} and A_{2B} are Analogue Devices 48J and AD528, respectively. *B*, *C*, bode magnitude asymptotes for the amplifiers (upper curves) and preparation (lower curves). *B*, potentiometric loop. Z_{A1} is the transfer impedance of A_1; Y_{AC} is the transfer admittance between electrodes *A* and *C* at rest. The dashed line shows the effect of maximum membrane conductance, and the dotted line represents the effect of the stray capacitance C_{AC}. *C*, transfer functions of the voltage clamp amplifier T_{A2} and the transfer function T_{EA} between *E* and *A*, including the action of A_1. The dashed line again shows the effect of maximum membrane conductance. The dotted line shows the limitation on T_{A2} placed by the stray capacitance, C_{EC}.

Design of the series resistance compensation network

Hodgkin, Huxley & Katz (1952) introduced the now widely-used series compensation technique, which consists of adding a portion of the current monitor signal to the voltage-clamp command voltage. Since this addition constitutes positive feed-back, it tends to destabilize the voltage clamp, often causing oscillation when only a fraction of the series resistance has been compensated. The theory will be presented here for the design of series resistance compensation networks that have only small effects on clamp stability, while allowing all of the series resistance to be compensated. The actual network used in the present voltage clamp circuit will then be described.

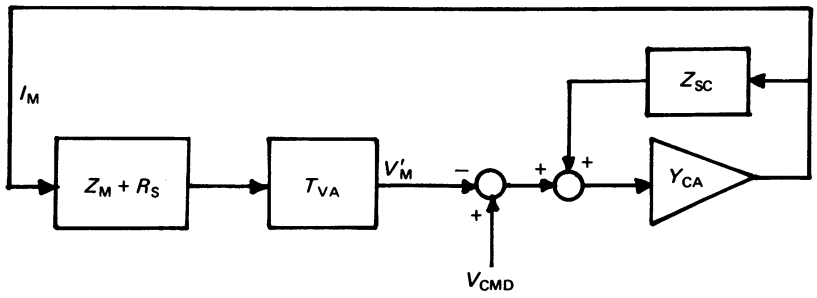

Fig. 14. Block diagram of a general voltage-clamp circuit with series resistance compensation. The voltage measuring circuitry with transfer function T_{VA} provides an estimate V'_M of the membrane potential, distorted by T_{VA} and the effect of the series resistance R_S. V'_M is compared with the command voltage V_{CMD} and the error is converted to an injected current I'_M by the clamp amplifier, Y_{CA}. The series resistance network Z_{SC} perturbs the error signal according to the injected current. It constitutes a positive feed-back path around the clamp amplifier.

A block diagram of a general voltage-clamp circuit is shown in Fig. 14. The various transfer functions Z_M, R_S, T_{VA}, Y_{CA} and Z_{SC} are the Laplace transforms of the impulse responses of the membrane impedance, series resistance, voltage monitor, clamp amplifier, and compensation network, respectively. The actual membrane potential response to the Laplace-transformed current $I_M(s)$ is

$$V_M(s) = Z_M(s)I_M(s) \tag{A 1}$$

The response of the *observed* membrane potential V'_M is different. It is the sum of membrane and series resistance components, and is modified by the transfer function of the voltage measuring circuitry T_{VA}:

$$V'_M = (Z_M + R_S)\, T_{VA} I_M \tag{A 2}$$

T_{VA} is ideally unity at all frequencies, but in practice its magnitude decreases at high frequencies.

The clamp amplifier provides a membrane current I_M in response to the difference between V'_M and the command voltage V_{CMD} according to its transfer function Y_{CA}. When the series resistance compensation Z_{SC} is included, I_M is given by

$$I_M = (V_{CMD} - V'_M + Z_{SC} I_M)\, Y_{CA} = (V_{CMD} - V'_M) \frac{Y_{CA}}{1 - Y_{CA} Z_{SC}} \tag{A 3}$$

Substituting (A 3) into (A 2) we obtain the response in V'_M to the command signal:

$$\frac{V'_M}{V_{CMD}} = \frac{T_{VA} Y_{CA} (Z_M + R_S)}{1 + Y_{CA}(T_{VA} Z_M + T_{VA} R_s - Z_{SC})} \tag{A 4}$$

If $Z_{SC} = 0$, $T_{VA} \to 1$ and $Y_{CA} \to^{\infty}$ then V'_M follows the command exactly. However, the actual membrane potential

$$V_M = \frac{Y_{CA} Z_M V_{CMD}}{1 + Y_{CA} (T_{VA} Z_M + T_{VA} R_s - Z_{SC})} \tag{A 5}$$

is nevertheless in error, with $V_M \cong V_{CMD} Z_M/(Z_M + R_s)$. If instead $Z_{SC} = T_{VA} R_s$, then V_M would follow the command exactly.

Since T_{VA} typically deviates from unity at high frequencies, it is important that Z_{SC} show a frequency dependence. Otherwise, when $|Z_{SC}| \geqslant |T_{VA}\,(Z_m + R_s)|$ at high frequencies, the voltage clamp will oscillate. The frequency where the size of $|Z_{SC}|$ is most important is the loop closure frequency, where $|Y_{CA}\, T_{VA}\, (Z_m + R_s)| = 1$. If Z_{SC} is made to be small relative to $T_{VA} R_s$ at this frequency, the transient response and stability of the clamp will be little affected by the series resistance compensation.

A very conservative design was used for Z_{sc} in the voltage clamp described here. T_{VA}, which in the case of the node of Ranvier voltage clamp describes the A pool voltage in response to the membrane potential, was approximately described by the second-order low-pass function

$$T_{VA}(s) \cong \frac{\omega_o^2}{s^2 + 1{\cdot}4\, \omega_o s + \omega_o^2}$$

where the natural frequency ω_o was of the order of $10^6\ \mathrm{sec}^{-1}$. The loop closure frequency ω_c of the voltage clamp was typically $3 \times 10^5\ \mathrm{s}^{-1}$. The form of Z_{sc} was chosen to be

$$Z_{sc} = \frac{R_{sc}}{(\tau s + 1)\,(\tau s/3 + 1)} \tag{A 6}$$

where R_{sc} is set by a potentiometer. The time constant $\tau = 10\ \mu\mathrm{sec}$, so that $[Z_{sc}] \cong \frac{1}{4}[R_s T_{VA}]$ at the loop closure frequency $s = i\omega_o$.

The relatively long time-constant τ allows the compensation to have only a small destabilizing effect on the voltage clamp. It does mean, however, that the series resistance is compensated only for time scales on the order of τ or longer. For shorter times the series resistance is effectively uncompensated. Since the series resistance in the frog node of Ranvier is relatively small, this transient error was not a problem in the experiments reported here.

Resistance measurement

The voltage clamp system included circuitry for the indirect measurement of the internodal resistances of the preparation R_{ED} and R_{CD}, the seal resistance R_{BC} and the resting membrane resistance R_M. For convenience the equations describing the measurement of these resistances will be written in terms of their reciprocals, the

conductances G_{ED}, G_{CD}, G_{BC} and the resting membrane conductance G_M. To determine the values of these four quantities, four independent measurements are made. Three of the measurements are of the current change in C pool due to small voltage perturbations in each of the other three pools, with the voltages at the remaining pools held constant:

$$Y_{BC} = \frac{\partial I_C}{\partial V_B}$$

$$Y_{AC} = \frac{\partial I_C}{\partial V_A} = \frac{G_{CD} G_M}{G_{CD} + G_{ED} + G_M} \tag{A 7}$$

$$Y_{EC} = \frac{\partial I_C}{\partial V_E} = \frac{G_{ED} G_{CD}}{G_{CD} + G_{ED} + G_M}$$

The fourth measurement requires that the membrane conductance be changed; this was accomplished by activating either the sodium or potassium conductance. The method used in all the experiments reported here relies on the presence of the sodium current. An action potential is elicited by a short negative pulse applied to the A pool; after the stimulating pulse the evoked currents I_C and I_E are measured simultaneously. Their ratio provides the fourth relation,

$$\frac{\delta I_E}{\delta I_C} = \frac{G_{ED}}{G_{CD}} \tag{A 8}$$

A second method involves depolarizing the membrane to activate the membrane potassium conductance. It was used as an independent check in a few experiments. During the last 200 ms of 300 ms depolarizations to 0 mV the response of I_C to perturbations in V_A and V_E was measured

$$Y'_{AC} = \frac{\partial I'_C}{\partial V_A} = \frac{G_{CD} G'_M}{G_{CD} + G_{ED} + G'_M}$$

$$Y'_{EC} = \frac{\partial I'_C}{\partial V_E} = \frac{G_{CD} G_{ED}}{G_{CD} + G_{ED} + G'_M} \tag{A 9}$$

The introduction of a fifth unknown parameter, the altered membrane conductance G'_M, requires a total of five relations to be satisfied. The four equations (A 7) and (A 8) or five equations (A 7) and (A 9) are readily solved to give expressions for the unknown parameters in terms of the measured admittances.

Chiu, Ritchie, Rogart & Stagg (1979) used a simplified version of this method to measure the resistances. They destroyed the nodal membrane at the end of each experiment, making G'_M very large. In this case eqn. (A 9) simplify to $Y'_{AC} = G_{CD}$ and $Y_{EC} = 0$.

The circuitry that performs the resistance measurement is shown in Fig. 15. The perturbing signal is a 100 Hz sine wave which is applied to the various electrodes through MOS analogue switches. I_C is monitored by amplifier A_{1A} (see Fig. 13) which for this purpose has an added 10^8 Ω feed-back resistor. A similar circuit is used to monitor I_E. The filtered current signals and a reference signal are sampled by an A–D converter. The computer performs synchronous detection on 20 cycles of the

I_C signal by multiplying it by the reference and then calculates the various conductances. Only the real parts of the admittances are measured, and the frequency of the perturbing signal was chosen to be small compared to G_M/C so that the membrane capacitance would have a negligible effect on the estimate of G_M. The frequency was also chosen to be large compared to τ_n^{-1}, the characteristic rate of the voltage-dependent potassium conductance. The amplitude of the signal is 2 mV r.m.s., chosen small to avoid nonlinear effects of the potassium conductance but

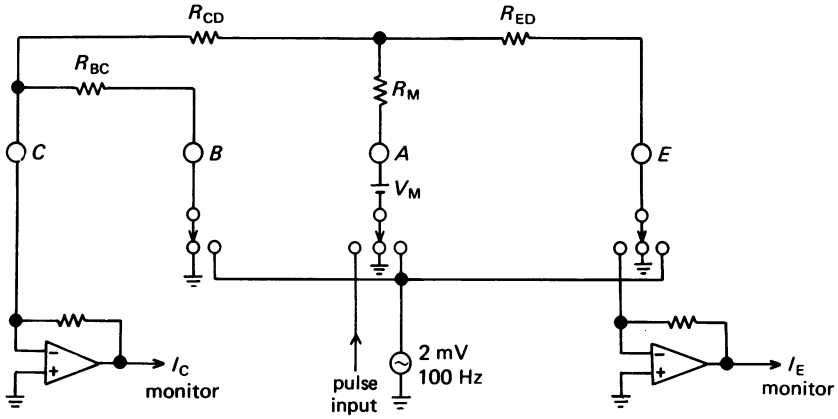

Fig. 15. Resistance measurement circuitry. Solid-state analogue switches allow the *B*, *A* and *E* electrodes to be connected to a 100 Hz sine-wave signal or to ground. Electrode *A* can also receive a stimulus pulse to elicit an action potential. The currents at *C* and *E* are monitored by current-to-voltage converters having feed-back resistances of 10^8 and 10^7 Ω, respectively. (The currents through the *A*–*E* leakage pathway preclude the use of a higher resistance at *E*, while at *C* the large resistance allows low noise measurements.) The current monitor signals are band-pass filtered and digitized for computer processing.

large enough to give a typical precision of 10^{-10} S in the measurement of admittances in eqn. (A 7). Successive determinations of the resistance values usually differed by less than 3 %, and values from the two measurement methods agreed within 10 % on those fibres where potassium currents were not blocked by internal Cs^+ and both methods could be used.

REFERENCES

ARMSTRONG, C. & BEZANILLA, F. (1977). Inactivation of the sodium channel II. Gating current experiments. *J. gen. Physiol.* **70**, 567–590.

BEGENESICH, T. & STEVENS, C. F. (1975). How many conductance states do potassium channels have? *Biophys. J.* **15**, 843–846.

BLAIR, E. & ERLANGER, J. (1932). Responses of axons to brief shocks. *Proc. Soc. exp. Biol. Med.* **29**, 926–927.

CHANDLER, W. K. & MEVES, H. (1970). Evidence for two types of sodium conductance in axons perfused with sodium fluoride solution. *J. Physiol.* **211**, 653–678.

CHIU, S. Y. (1977). Inactivation of sodium channels: second order kinetics in myelinated nerve. *J. Physiol.* **273**, 573–596.

CHIU, S. Y., RITCHIE, J. M., ROGART, R. B. & STAGG, D. (1979). A quantitative description of membrane currents in rabbit myelinated nerve. *J. Physiol.* **292**, 149–166.

CONTI, F., DEFELICE, L. J. & WANKE, E. (1975). Potassium and sodium ion current noise in the membrane of the squid giant axons. *J. Physiol.* **248**, 45–82.

CONTI, F. & WANKE, E. (1975). Channel noise in nerve membranes and lipid bilayers. *Q. Rev. Biophys.* **8**, 451–506.

CONTI, F., HILLE, B., NEUMCKE, B., NONNER, W. & STÄMPFLI, R. (1976*a*). Measurement of the conductance of the sodium channel from current fluctuations at the node of Ranvier. *J. Physiol.* **262**, 699–727.

CONTI, F., HILLE, B., NEUMCKE, B., NONNER, W. & STÄMPFLI, R. (1976*b*). Conductance of the sodium channel in myelinated nerve fibres with modified sodium inactivation. *J. Physiol.* **262**, 728–742.

DEFELICE, L. J. (1977). Fluctuation analysis in neurobiology. *Int. Rev. Neurobiol.* **20**, 169–208.

DERKSEN, H. E. (1965). Axon membrane voltage fluctuations. *Acta physiol. pharmacol. neerl.* **13**, 373–466.

DODGE, F. & FRANKENHAEUSER, B. (1958). Membrane currents in isolated frog nerve fibre under voltage clamp conditions. *J. Physiol.* **143**, 76–90.

DODGE, F. & FRANKENHAEUSER, B. (1959). Sodium currents in the myelinated nerve fibre of *Xenopus laevis* investigated with the voltage clamp technique. *J. Physiol.* **148**, 188–200.

DROUIN, H. & NEUMCKE, B. (1974). Specific and unspecific charges at the sodium channels of the nerve membrane. *Pflügers Arch.* **351**, 207–229.

EHRENSTEIN, G., LECAR, H. & NOSSAL, R. (1970). The nature of the negative resistance in bimolecular lipid membranes containing Excitability-Inducing Material. *J. gen. Physiol.* **55**, 119–133.

ERLANGER, J., BLAIR, E. & SCHOEPFLE, G. (1941). A study of the spontaneous oscillations in the excitability of nerve fibres, with special reference to the action of strychnine. *Am. J. Physiol.* **351**, 207–229.

FOX, J. M. (1976). Ultra-slow inactivation of the ionic currents through the membrane of myelinated nerve. *Biochim. biophys. Acta* **426**, 245–257.

FRANKENHAEUSER, B. & MOORE, L. E. (1963). The effect of temperature on the sodium and potassium permeability changes in myelinated nerve fibres of *Xenopus laevis*. *J. Physiol.* **169**, 431–437.

GOLDMAN, D. (1943). Potential, impedance, and rectification in membranes. *J. gen. Physiol.* **27**, 37–60.

HILL, T. L. & CHEN, Y. (1972). On the theory of ion transport across the nerve membrane. IV. Noise from the open-close kinetics of K^+ channels. *Biophys. J.* **12**, 948–959.

HILLE, B. (1967). The selective inhibition of delayed potassium currents in nerve by tetraethylammonium ion. *J. gen. Physiol.* **50**, 1287–1302.

HILLE, B. (1971*a*). The permeability of the sodium channel to organic cations in myelinated nerve. *J. gen. Physiol.* **58**, 599–619.

HILLE, B. (1971*b*). Voltage clamp studies on myelinated nerve fibres. In *Biophysics and Physiology of Excitable Membranes*, ed. ADELMAN, W. J., JR. New York: van Nostrand Reinhold.

HODGKIN, A. L., HUXLEY, A. F. & KATZ, B. (1952). Measurement of current-voltage relations in the membrane of the giant axon of *Loligo*. *J. Physiol.* **116**, 424–448.

LAMB, T. D. & SIMON, E. J. (1977). Analysis of electrical noise in turtle cones. *J. Physiol.* **272**, 435–468.

LECAR, H. & NOSSAL, R. (1971*a*). Theory of threshold fluctuations in nerves. I. Relationship between electrical noise and fluctuations in axon firing. *Biophys. J.* **11**, 1048–1067.

LECAR, H. & NOSSAL, R. (1971*b*). Theory of threshold fluctuations in nerves. II. Analysis of various sources of membrane noise. *Biophys. J.* **11**, 1068–1084.

MAURO, A., CONTI, F., DODGE, F. & SCHOR, R. (1970). Subthreshold behavior and phenomenological impedance of the squid giant axon. *J. gen. Physiol.* **55**, 497–523.

MONNIER, A. & JASPER, H. (1932). Recherche de la rélation entre les potentiels d'action élémentaires et la chronaxie de subordination. Nouvelle demonstration du fonctionnement par 'tout ou rien' de la fibre nerveuse. *C. r. Soc. Biol., Paris* **110**, 547–549.

NEHER, E. & SAKMANN, B. (1976). Single-channel currents recorded from membrane of denervated frog muscle fibres. *Nature, Lond.* **260**, 779–802.

NEHER, E., SAKMANN, B. & STEINBACH, J. H. (1978). The extracellular patch-clamp: a method

for resolving currents through individual open channels in biological membranes. *Pflügers Arch.* **375**, 219–228.

NEHER, E. & STEVENS, C. F. (1977). Conductance fluctuations and ionic pores in membranes. *A. Rev. Biophys. Bioeng.* **6**, 345–381.

NEUMCKE, B., SCHWARZ, W. & STÄMPFLI, R. (1979). Slow actions of hyperpolarization on sodium channels in the membrane of myelinated nerve. *Biochim. biophys. Acta* **558**, 113–118.

NONNER, W. (1969). A new voltage clamp method for Ranvier nodes. *Pflügers Arch. ges. Physiol.* **309**, 176–192.

PECHER, C. (1932). La fluctuation d'excitabilité de la fibre nerveuse. *Archs int. Physiol.* **49**, 129–152.

POUSSART, D. (1971). Membrane current noise in lobster axon under voltage clamp. *Biophys. J.* **11**, 211–234.

SIGWORTH, F. (1977). Sodium channels in nerve apparently have two conductance states. *Nature, Lond.* **270**, 265–267.

SIGWORTH, F. (1978). Fraction of sodium channels open at peak conductance. *Biophys. J.* **21**, 41*a*.

SIGWORTH, F. (1980). The conductance of sodium channels under conditions of reduced current at the node of Ranvier. *J. Physiol.* **307**, 131–142.

STÄMPFLI, R. & HILLE, B. (1976). Electrophysiology of the peripheral myelinated nerve. In *Frog Neurobiology*, ed. LLINAS, R. & PRECHT, W. New York: Springer-Verlag.

VAN DEN BERG, R. J. (1978). *Electrical Fluctuations in Myelinated Nerve Membrane.* Thesis, Leiden.

VERVEEN, A. (1961). *Fluctuation in Excitability.* Amsterdam: Drukkerij Holland N.V.